HHS Public Access

Author manuscript

Brain Imaging Behav. Author manuscript; available in PMC 2020 May 08.

Regional Growth Trajectories of Cortical Myelination in Adolescents and Young Adults: Longitudinal Validation and Functional Correlates

Dongjin Kwon[1,2], **Adolf Pfefferbaum**[1,2], **Edith V. Sullivan**[1], and **Kilian M. Pohl**[2,*]

[1]Department of Psychiatry and Behavioral Sciences, Stanford University, Stanford, CA

[2]Center for Health Sciences, SRI International, Menlo Park, CA

Abstract

Adolescence is a time of continued cognitive and emotional evolution occurring with continuing brain development involving synaptic pruning and cortical myelination. The hypothesis of this study is that heavy myelination occurs in cortical regions with relatively direct, predetermined circuitry supporting unimodal sensory or motor functions and shows a steep developmental slope during adolescence (12-21 years) until young adulthood (22- 35 years) when further myelination decelerates. By contrast, light myelination occurs in regions with highly plastic circuitry supporting complex functions and follows a delayed developmental trajectory. In support of this hypothesis, cortical myelin content was estimated and harmonized across publicly available datasets provided by the National Consortium on Alcohol and NeuroDevelopment in Adolescence (NCANDA) and the Human Connectome Project (HCP). The cross-sectional analysis of 226 no-to-low alcohol drinking NCANDA adolescents revealed relatively steeper age-dependent trajectories of myelin growth in unimodal primary motor cortex and flatter age-dependent trajectories in multimodal mid/posterior cingulate cortices. This pattern of continued myelination showed smaller gains when the same analyses were performed on 686 young adults of the HCP cohort free of neuropsychiatric diagnoses. Critically, a predicted correlation between a motor task and myelin content in motor or cingulate cortices was found in the NCANDA adolescents, supporting the functional relevance of this imaging neurometric. Furthermore, the regional trajectory slopes were confirmed by performing longitudinally consistent analysis of cortical myelin. In conclusion, coordination of myelin content and circuit complexity continues to develop throughout adolescence, contributes to performance maturation, and may represent active cortical development climaxing in young adulthood.

[*]**Correspondence** Kilian M. Pohl, Ph.D., Center for Health Science, SRI International, 333 Ravenswood Avenue, Menlo Park, CA 94025, USA, phone: (831) 247 2275, FAX: (650) 859-2743, kilian.pohl@sri.com.

Conflict of interest. None of the authors have conflicts of interest with the reported data or their interpretation.

Ethical approval: All procedures performed in studies involving human participants were in accordance with the ethical standards of the institutional and/or national research committee and with the 1964 Helsinki declaration and its later amendments or comparable ethical standards.

Informed consent: Informed consent was obtained from all individual participants included in the study.

Keywords

cortical myelin; development; adolescence; early adulthood

1 Introduction

Myelin is a fatty sheath composed primarily of oligodendrocyte glycoprotein that insulates the axon and enhances speed and fidelity of neural signal transmission (Tomassy et al. 2016). While myelinated fibers are the main component of brain white matter, significant amounts of myelin are distributed in the gray matter with myelination patterns defining the cortical myeloarchitecture determined from postmortem study (Nieuwenhuys 2013). Over the last decade, a growing number of *in vivo* MRI studies report converging findings with postmortem patterns of myelination that continues throughout adolescence and into young adulthood (Miller et al. 2012; Nieuwenhuys 2013). Untapped to date is the analysis of multi-site, multimodal, *in vivo* human neuroimaging data to approximate regional cortical myelin content throughout the adolescent years and into young adulthood. Accordingly, the current analysis addressed this lacuna by estimating cortical myelin of healthy, non-substance misusing adolescents using MRIs from the National Consortium on Alcohol and NeuroDevelopment in Adolescence (NCANDA) study (Brown et al. 2015; Pfefferbaum et al. 2016; Sullivan et al. 2016) and of healthy young adults using comparable data from Human Connectome Project (HCP) (Van Essen et al. 2013).

The timing and density of cortical myelin development modulate functions. Cortical circuits that become heavily myelinated are suited for speed of sensory and motor processing, whereas lightly myelinated circuits serve higher-order, cognitive functions (Glasser et al. 2014; Glasser et al. 2016) that continue maturation throughout adolescence and into young adulthood (Sowell et al. 2003). Critically, the adolescent years have the highest prevalence for the initial expression of psychotic and psychopathic episodes and for the greatest vulnerability to environmental influences, such as from alcohol and drug consumption initiation (Bava and Tapert 2010). These conditions are related to disturbance of cortical structure and function that either cause maldevelopment of cortical ultrastructure or result from trajectory deviations in development (Squeglia et al. 2015). Indeed, the cortical myelination process may also participate in synaptic development thought to continue through these ages (Jernigan et al. 1991; Miller et al. 2012).

Recent technological advances have introduced the potential for non-invasively identifying and tracking normal and abnormal development of cortical myelin *in vivo*. These technologies assume that MRI-based signals across the cortical gray matter mirror myelin content. This myelin-inclusive signal is assessed by optimizing T1-weighted protocols for intracortical dynamic ranges (Bock et al. 2009; Bock et al. 2013; Fischl et al. 2004; Lutti et al. 2014; Rowley et al. 2017), modeling the short T2 relaxation component for water trapped between myelin sheaths using multi-echo T2 maps (Arshad et al. 2017; MacKay et al. 1994; Whittall et al. 1997), or computing the ratio of T1-weighted and T2-weighted MRIs (Ganzetti et al. 2014; Glasser and Van Essen 2011; Glasser et al. 2013; Glasser et al. 2014; Grydeland et al. 2013; Grydeland et al. 2016; Shafee et al. 2015). Computing the ratio based

on common T1-weighted and T2-weighted MRI acquisition protocols (Glasser and Van Essen 2011; Glasser et al. 2013; Glasser et al. 2014) lays the foundation for repurposing existing MRI data to estimate the temporal order of normal regional cortical development throughout adolescence to maturity (Casey et al. 2000; Stiles and Jernigan 2010). The repurposing is possible as the lipids composing about 70% of myelin are a dominant source of T1-weighted and T2-weighted MRI contrasts in brain tissue (Leuze et al. 2017). A postmortem study (Miller et al. 2012) has shown that the age-dependent slope of this unitless metric is specific to individual regions.

In this report, MRIs of 226 healthy adolescents from the NCANDA study and 686 young adults from the HCP study are repurposed to characterize the developmental trajectory of regional myelin density from adolescence to adulthood. Accordingly, the estimate of myelin contents across these two large, publicly-available datasets were harmonized so that myelin scores of the HCP data set were similar to those provided by the original study. We predicted that heavy myelination occurs in cortical regions with relatively direct, predetermined circuitry supporting unimodal sensory or motor functions and shows a steep developmental slope until young adulthood when further myelination decelerates (for example, area 4). By contrast, light myelination occurs in regions with highly plastic circuitry supporting complex functions (for example, areas 23/24) and follows a temporally lagging developmental trajectory. For the NCANDA cohort, functional ramifications of the regionally different myelin contents were tested with a speeded, eye-hand coordination test. Further, longitudinal NCANDA data were used to validate the cross-sectionally observed developmental trajectories. To do so, our approach harmonized the computations of myelin content across visits by matching the intensities of the MRIs of the follow up visits to the baseline so that they agreed with respect to the low-frequency patterns. This procedure reduced the variance in myelin content across visits, which was verified on human phantom data. Of those regions with significant-age effects, permutation testing identified those whose myelin scores significantly correlated with the performance scores of an eye-hand coordinated, speeded motor task. In summary, this analysis makes three novel contributions: (1) characterizing the age-related pattern of cortical myelin content in 992 individuals aged 12 to 35 years, harmonized across two independently-collected data sets; (2) demonstrating the relation between regional developmental trajectories of myelin content and brain function in youth aged 12 to 21 years; (3) and developing longitudinally consistent analysis of myelin content thereby confirming the adolescent developmental patterns of myelin content of the cross-sectional study.

2 Methods

2.1 Participants

The longitudinal data of the NCANDA Release (NCANDA_PUBLIC_2Y_STRUCTURAL_V02), which was made available through the Scalable Informatics for Biomedical Imaging Studies (Muller-Oehring et al. 2017; Nichols and Pohl 2015; Pfefferbaum et al. 2016; Pohl et al. 2016; Rohlfing et al. 2014) (sibis.sri.com), included 226 adolescents (108 male; 118 female) aged 12 to 21 years. These participants were recruited by the University of Pittsburgh (N=90; site P) and the Oregon

Health and Sciences University (N=136; site O), and their demographic information is summarized in Table 1. They met no-to-low alcohol and drug use criteria (Brown et al. 2015), **urine screening on the day of scanning confirmed the absence of recreational drug use,** and were scanned on Siemens MRI systems as recommended for myelin mapping (Glasser et al. 2014). 32 participants were ambidextrous (Edinburgh handedness questionnaire (Oldfield 1971)) and of the remaining 194 adolescents Grooved Pegboard Test were administrated separately for each hand (Lafayette-Instrument 2002). All participants underwent an informed consent process with a research associate trained in human subject research protocols. Adult participants provided written informed consent as did the parents of minor participants before engaging in the study. Minor participants provided assent before participation. The Internal Review Boards of each site approved this study, and each site followed this procedure to obtain voluntary informed consent or assent, depending on the age of the participant. **The follow-up rate of Year 2 was 82% (N=185), which was not impacted by age, sex, ethnicity, and site ($p<0.05$; two sample t-test). Of those 185 participants, 177 of them had 3 MRI scans with 1.03 years being the average time between acquisitions**.

The Data Release S900 of the Human Connectome Project (HCP) (downloaded from https://db.humanconnectome.org) consisted of single visits of 897 young adults age 21 to 35 years. All participants underwent an informed consent process. The Washington University Institutional Review Board approved subject recruitment procedures, informed consent forms, and data collection and dissemination. Our analysis excluded one subject whose DSM-IV (American Psychiatric Association 2000) scores were incomplete, one due to missing twin zygosity information (required to define exchangeability blocks for permutation tests), and 209 individuals who met DSM-IV alcohol abuse, alcohol dependence, or marijuana dependence criteria. The remaining 686 young adults comprised data from 264 male and 422 female participants.

2.2 Data Releases

For each participant, the NCANDA release provided demographic information, Grooved Pegboard Test scores (Lafayette-Instrument 2002), measuring dexterity and eye-hand coordinated movement, and structural MRIs acquired in the sagittal plane on 3T Siemens Trio Tim scanners using a 12-channel head coil. T1-weighted MRIs were acquired using the gradient-echo MPRAGE sequence (TR = 1900ms, TI = 900ms, TE = 2.92ms, flip angle = 9°, matrix = 256×256, FOV = 24cm, slice dimensions = 0.9375×0.9375×1.2mm, 160 slices). T2-weighted MRIs were acquired using the spin-echo SPACE sequence (TR = 3200ms, TE = 404ms, *variable flip angle*, matrix = 512×512, FOV = 24cm, slice dimensions = 0.46875×0.46875×1.2mm, 160 slices, GRAPPA acceleration = 2).

The structural MRIs of each young adult of the HCP release were acquired on a **single** 3T Siemens Skyra scanner with a 32-channel head coil **and housed at Washington University in St Louis** (Glasser et al. 2013). T1-weighted MRIs were acquired using the gradient-echo MPRAGE sequence (TR = 2400ms, TI = 1000ms, TE = 2.14ms, flip angle = 8°, matrix = 320×320, FOV = 22.4cm, slice dimensions = 0.7×0.7×0.7mm, 256 slices). T2-weighted MRIs were acquired using the spin-echo SPACE sequence (TR = 3200ms, TE = 565ms,

variable flip angle, matrix = 320×320, FOV = 22.4cm, slice dimensions = 0.7×0.7×0.7mm, 256 slices, GRAPPA acceleration = 2).

2.3 Data Processing

2.3.1 NCANDA-Specific Pre-processing Pipeline—For each NCANDA MRI baseline visit, preprocessing involved noise removal (Coupe et al. 2008), correcting field inhomogeneity via N4ITK (Version: 2.1.0) (Tustison et al. 2010), aligning T2-weighted to T1-weighted MRI using CMTK (Version: 3.2.3) (Rohlfing and Maurer 2003). A brain mask was defined through majority voting (Rohlfing et al. 2004) across the maps extracted from bias and non-bias corrected T1-weighted and T2-weighted MRIs via FSL BET (Version: 5.0.6) (Smith 2002), AFNI 3dSkullStrip (Version: AFNI_2011_12_21_1014) (Cox 1996), FreeSurfer's mri_gcut (Version: 5.3.0) (Sadananthan et al. 2010), and ROBEX (Version: 1.2) (Iglesias et al. 2011). The mean curvature along cortical surface, white matter boundary, and pial surface of the resulting skull-stripped T1-weighted MRI was extracted by FreeSurfer (Version: 5.3.0) (Dale et al. 1999; Fischl et al. 1999; Fischl 2012). Skull-stripping was further refined by aligning the white matter boundary to the T2-weighted MRIs via FSL epi_reg (Version: 5.0.6) and removing voxels with low T2-weighted intensities near the pial surface.

2.3.2 Computing Longitudinally-Consistent Myelin Scores—The refined skull-stripped T1-weighted MRIs were then analyzed by FreeSurfer to measure supratentorial volume, refine the pial surface, and extract the midthickness surface accompanied with T1-weighted and T2-weighted intensities. Each modality was mapped from the volume to the surface space using the HCP approach based on the Connectome Workbench (Version: 1.2.3) (Glasser et al. 2013), i.e., for each vertex of the *midthickness* surface the average intensity value with respect to a cylinder centered on that vertex was computed. A 14.14 mm Gaussian filter kernel was also applied to those intensity values to extract their *low frequency patterns*.

For each follow-up visit, noise removal (Coupe et al. 2008) was applied to the corresponding MRIs, which were then non-rigidly registered to their baseline modality using ANTs (Version: 2.1.0) (Avants et al. 2008). The midthickness surface of the baseline was then used to record the initial MRI intensity and low frequency values at each vertex of that follow-up scan using again the HCP mapping procedure. To improve longitudinal consistency of our analysis, the multiplicative inhomogeneity (Sled et al. 1998) of the MRI intensity values on the surface were then matched to that of the baseline by computing at each vertex the ratios between the low-frequency values at baseline and follow-up, and applying that ratio to the MRI intensity values of the follow-up scan. The reliability of myelin content from this approach (called the *longitudinal* approach) was compared with that of the myelin content estimated independently for each visit (called the *cross-sectional* approach).

For each time point, the *raw* myelin content at each vertex along the midthickness surface was defined by the ratio between the T1-weighted and T2-weighted intensity values of that vertex. In line with HCP processing (Glasser et al. 2013), the *normalized* myelin content was then computed in order to compare the myelin content across subjects. Specifically, the brain

surface containing the *raw* myelin content was mapped to the 2mm HCP template by aligning *sulc* features (i.e., average convexity) using multimodal surface matching (Robinson et al. 2014). The *raw* myelin scores on the 2mm HCP template were then modified so that their corresponding *low frequency pattern* (i.e., the output of a 14.14 mm Gaussian filter kernel applied to the vertex-wise values) matched the one of the average myelin content across the Conte69 subjects (the *reference* myelin content) (Glasser and Van Essen 2011). Doing so normalized the distribution of the resulting *normalized* myelin content to the reference myelin content. The *normalized* myelin content of the cross-sectional HCP data set was computed by first resampling their skull-stripped, inhomogeneity corrected, structural MRIs to match the resolution of the MRIs of NCANDA (1.2×0.9375×0.9375mm) and then following the procedure for computing *normalized* myelin content.

2.4 Group Analysis

2.4.1 Identifying Cohort-specific Developmental Patterns—Separately for each cohort, our analysis identified developmental patterns in myelin by measuring the age effects at each vertex of the template. To do so, a general linear model was fitted to the baseline myelin content viewing **age** as a predictor and **sex** (female/male), **ethnicity** (Caucasian/African-American/Others), **svol** (supratentorial volume in cc), and **site** (NCANDA collection sites; omitted in HCP analysis) as confounding factors for each subject **s**,

$$\mathbf{myelin_s} \sim \beta_0 + \beta_{\text{age}} \cdot \mathbf{age_s} + \beta_{\text{sex}} \cdot \mathbf{sex_s} + \beta_{\text{ethnicity}} \cdot \mathbf{ethnicity_s} + \beta_{\text{svol}} \cdot \mathbf{svol_s} + \beta_{\text{site}} \cdot \mathbf{site_s}.$$

From that model, family-wise error rate (FWER)-corrected P-values were inferred via permutation testing through PALM (Version: a103; iterations: 5000; one-sided P values) (Winkler et al. 2014). Clusters of vertices with significant age effects ($P < 0.01$) were identified by PALM's threshold-free cluster enhancement approach (TFCE; Parameters: H=2, E=1, C=26). The chosen significance threshold ($P < 0.01$) was more conservative than for the remaining experiments ($P < 0.05$) to focus the discussion on only highly correlated age-related findings. Cross-sectional age differences were visualized by the vertex-wise β_{age} values. Those computations were repeated with respect to the *normalized* myelin content scores averaged over the regions defined by the HCP multimodal parcellation atlas (MMP 1.0) (Glasser et al. 2016) consisting of 180 areas per hemisphere.

On the NCANDA data set, the post-hoc analysis of regions with significant age-effects consisted of relating the normalized myelin content of those regions to the neuropsychological testing and confirming the development patterns through longitudinal analysis.

2.4.2 Neuropsychological Testing—For each region with significant age effects, the average regional *normalized* myelin content was tallied over vertices in that region whose β_{age} value agreed with the significant finding, e.g., β_{age} of a vertex and region indicated a positive age effect. The resulting myelin score was then correlated with the Grooved Pegboard Test scores (time in seconds needed to complete the test) (Lafayette-Instrument 2002) separately for the dominant and non-dominant hand of the 194 non-ambidextrous adolescents (right handed=180; left handed=14). To identify significant correlations (P-value

< 0.05), a linear regression model removed the confounding factors of age, sex, svol, site, ethnicity, and handedness from the regional myelin and performance scores. The Pearson correlation 'r' between the corresponding residual scores was calculated for each region and hand. The P-value of 'r' was computed by Permutation testing (Boca et al. 2014) of the BRAVO toolbox V.2.0 (https://sites.google.com/site/bravotoolbox; iterations: 5000; one-sided t-test).

For the regions, whose average myelin content significantly correlated with the scores of the dominant hand, the regression on the original regional and performance scores was repeated with respect to all confounding factors but age. For each hand, a *Multiple Mediation Model* (Figure 1) examined the effect of age (independent variable) on the pegboard test scores (dependent variable) and identified which of two regional residual scores (intermediate variable) had a greater indirect effect, i.e., accounted for greater variance. The P-value of an effect was inferred from repeating the previous permutation test with respect to the normalized β_N value, which was the β value of the effect divided by the β value of the direct (unmediated) effect between age and the pegboard score.

2.4.3 Longitudinal Confirmation of Developmental Patterns—The longitudinal study of the *normalized* myelin content of the regions with significant age-related changes analyzed the *normalized* myelin content of **the 185 NCANDA adolescents that had longitudinal data from baseline to Year 2 (see** Table 1). For each of these regions, the age effects were estimated by fitting a linear mixed effects model (Bemal-Rusiel et al. 2013) with the fixed effects being **age** (age at baseline), **age^2**, **age*sex**, **sex**, **time** (time passed since baseline visit), **ethnicity**, **svol**, and **site**, and the random effects being **time** for each subject **s** and time point **t**

$$\mathbf{myelin}_{\mathbf{s},\mathbf{t}} \sim \beta_0 + \beta_{\text{age}} \cdot \mathbf{age}_{\mathbf{s}} + \beta_{\text{age2}} \cdot \mathbf{age}_{\mathbf{s}}^2 + \beta_{\text{age*sex}} \cdot \mathbf{age}_{\mathbf{s}} * \mathbf{sex}_{\mathbf{s}} + \beta_{\text{sex}} \cdot \mathbf{sex}_{\mathbf{s}} + \beta_{\text{time}} \cdot \mathbf{time}_{\mathbf{s},\mathbf{t}} + \beta_{\text{ethnicity}} \cdot \mathbf{ethnicity}_{\mathbf{s}} + \beta_{\text{svol}} \cdot \mathbf{svol}_{\mathbf{s}} + \beta_{\text{site}} \cdot \mathbf{site}_{\mathbf{s}} + b_{0s} + b_{1s} \cdot \mathbf{time}_{\mathbf{s},\mathbf{t}} \cdot$$

The direction, attenuation, and significance of the linear age effects β_{age} and quadratic age effects β_{age2} were reported (two-sided t-test; significant: P < 0.05).

3 Results

3.1 Age-dependent Differences in Cross-sectional Myelin Content in NCANDA Adolescents and HCP Young Adults

Our cortical myelin development hypothesis (shown as graphs in Figure 2) was supported by the cross-sectional trajectories of both the *raw* and *normalized* myelin content (see Appendix A.4). The *raw* myelin content was greater with age (ages 12 to 35) throughout the cortex; however, individual cortical regions differed with respect to age-dependent myelination trajectories. To highlight this difference, normalization of the raw myelin scores removed the growth pattern of the entire cortex so that a positive residual score (i.e., *normalized* myelin content) revealed greater myelin content and a negative normalized score encoded less myelin content relative to the myelin content of the entire cortex (Glasser et al. 2014). The resulting age-dependent myelination trajectories showed greater gains in myelin with age in

the motor cortex and smaller gains with age in the midcingulate cortex. These development patterns were more extreme (i.e., far larger or far smaller gains) during adolescence than in young adulthood.

This observation was also reflected in the age-dependent differences with respect to regression variable β_{age} of the *normalized* myelin content across the entire cortex. Figure 3*A* shows that the areas with greater gains (red) and lesser gains (blue) during adolescence (NCANDA) almost entirely disappeared during young adulthood (HCP). Furthermore, the significant vertex-wise (Figure 3*B*) and parcellated (Figure 3*C* age-dependent regions (shown in non-gray) were larger in the NCANDA adolescents than young HCP adults. During adolescence, greater gains in vertex-wise, *normalized* myelin content were significant (shown in red/yellow in Figure 3*B*) primarily in the primary motor cortex; lesser gains in the *normalized* myelin content (shown in blue/green) were located in the cingulate cortex, precentral sulcus, and insula cortex. Significant regional age-dependent differences (Figure 3*C* were observed in the primary motor cortex ([Brodmann] area 4) (Nieuwenhuys 2013) and cingulate cortex ([Vogt] areas 23c, p24', a24') (Vogt et al. 1995). Of those regions, areas 4 (left hemisphere) and p24' (right hemisphere) were also significantly different within the HCP young adults ($P < 0.05$) (Table 2 and Figure 4). However, with respect to areas 4, 23c, and p24', the corresponding age effects (β_{age}) measured in the NCANDA adolescent group were 1.3 to 2.9 times higher than those measured in the HCP young adults (Table 2 and Figure 4). For young adults, area 23c (right hemisphere) showed a trend towards an age effect ($P = 0.056$) (Table 2).

The more substantial gains during adolescence are also visualized by Figure 5, which plots the average *normalized* myelin content with respect to different ages of the NCANDA cohort. Areas in red have a greater and in blue a less myelin content relative to the entire cortex.

3.2 Relation between *Average Regional Normalized* Myelin Content and Grooved Pegboard Test Scores in NCANDA Adolescents

Faster Grooved Pegboard Test scores, measured as total time in seconds to complete the test, correlated with greater *normalized myelin* content. The correlation was significant (Table 3) for the left hemisphere when the test was executed with the dominant hand ($P = 0.009$) and for both hemispheres with respect to the non-dominant hand ($P = 0.013$ for the left and $P = 0.011$ for the right hemispheres). For area 23c and p24', faster time to pegboard completion time correlated with lower *normalized* myelin content (see also Figure 6). For area 23c, faster pegboard test scores of the non-dominant hand correlated with lower *normalized* myelin content ($P = 0.011$ for the left; $P = 0.027$ for the right hemisphere). For area p24', significant correlations were restricted to the right hemisphere for both dominant ($P = 0.013$) and non-dominant ($P = 0.001$) hands. In general, faster performance and greater myelin content were associated with older age of the adolescents.

For the average myelin content of areas 4 [L] and p24' [R] (where [L] denotes left and [R] denotes right), the multiple mediation model (Figure 1) measured the indirect effects, which are defined by the path from age to the regional myelin score (Figure 1, a_x) and from the regional myelin score to the pegboard score (Figure 1, b_x). The proportion of the indirect

effects of area 4 [L] was about twice as large as that of area p24' [R] for the dominant hand (28% for 4 [L] and 14% for p24' [R]) but had similar effects for the non-dominant hand (24% for 4 [L] and 22% for p24' [R]) (Table 4).

3.3 Longitudinal Validation Study in NCANDA Adolescents

Longitudinal analysis for upwards of three visits for each of 185 NCANDA adolescents (aged 12-21 years at baseline) confirmed the cross-sectional findings with respect to regions showing highly significant age effects on the *normalized* myelin content, namely, areas 4, 23c and p24' (Figure 7). As noted in Table 5, significant linear age effects were detected bilaterally for all three regions ($P < 0.05$ for all regions, where $P < 0.001$ for area 4 [R], 23c [R] and p24' [L]). A significant deceleration of the *normalized* myelin content increase was revealed for area 4 [R] ($P = 0.004$, $\beta_{age2} = -0.00017$) with the quadratic age effect (*i.e.*, with respect to β_{age2}) being negative while the gain with respect to the linear age effect (*i.e.*, with respect to β_{age}) was significantly greater than that of the entire cortex. The two regions with significant acceleration of aging effects (23c [R]: $P = 0.001$, $\beta_{age2} = 0.00013$; p24' [L]: $P = 0.022$, $\beta_{age2} = 0.00011$) had significantly smaller gains in *normalized* myelin content.

4 Discussion

Cortical myelin undergoes growth from pre-adolescence through young adulthood (Grydeland et al. 2013; Miller et al. 2012; Tomassy et al. 2016). Trajectories of the *normalized* myelin content (i.e., the myelin content normalized to the average Conte69 template) varied in the gain detected over several regions during adolescence. As displayed in Figure 3, the *normalized* myelin growth was spatially more homogenous across the entire cortex among young adults than adolescents, which may reflect the culmination of local intracortical circuitry development. Specific to adolescents, myelin developmental trajectories were relatively symmetrical by cerebral hemisphere and similar in male and female youth. Cortical myelin growth either had smaller gains (relative to the overall gain in myelin density of the cortex), as occurred in the mid and posterior cingulate cortices ([Vogt] areas p24' and 23c) supporting cognitive processes (Vogt et al. 1995), or greater gains, as occurred in the primary motor cortex ([Brodmann] area 4) supporting primary motor function (Nieuwenhuys 2013). Longitudinal data in the adolescents verified these cross-sectional slope patterns. Heterochronicity in cortical structural (Giedd et al. 2015; Raznahan et al. 2012; Shaw et al. 2008) and functional maturation (Fjell et al. 2012; Muller-Oehring et al. 2017; Stiles and Jemigan 2010) marked the continuation of neurodevelopment throughout adolescence and young adulthood and, as our analysis showed, includes cortical myelin and its functional ramifications in temporal, spatial, and density growth patterns. These findings are expanded next.

Regional Growth Trajectories of Cortical Myelin

Our analysis was based on estimating cortical myelin content from T1-weighted and T2-weighted MRIs taken from commonly acquired, multimodal MRI data results. This estimation is based on the observation that T1-weighted and T2-weighted MRIs show inversed MRI intensity relations for gray and white matter (Glasser and Van Essen 2011; Sigalovsky et al. 2006; Yoshiura et al. 2000), thus indicating that a ratio between T1-

weighted and T2-weighted MRIs can boost the myelin contrast while reducing the noise level. The analysis is advantageous over other *in vivo* studies, which had limited contrasts in lightly myelinated regions due to use of a single modality (Rowley et al. 2017), included the *raw* myelin content in analysis that potentially affected by the residual bias (Shafee et al. 2015), or had small samples to address questions about adolescent development (Grydeland et al. 2013).

Essential to the analysis was the harmonization of two large data sets collected in 912 healthy, young male and female participants in the NCANDA and HCP studies. Both the NCANDA and the HCP studies used very similar gradient-echo MPRAGE sequence for acquiring T1-weighted MRIs, which yielded excellent gray and white matter contrasts. Furthermore, data coordination involved use of the same processing steps and normalization of the myelin content across the data sets, which corrected for residual biases and made the mean of the *normalized* myelin content over the entire cortex similar across subjects. This approach for MRI processing substantially reduced variances in the estimate of myelin content (see Appendix A.4), thereby improving sensitivity to reveal selective differences in regional developmental patterns of myelin content. **The processing did not, however, normalize the variance across the two data sets, which was much larger for the HCP data set (see Figure 4), and most likely caused by their discrepancy in T2-weighted MRI acquisition.** Critically, the cross-sectional results reported herein were verified with respect to the young adults on the original MRIs provided by HCP (i.e., 0.7mm isotropic resolution; see Appendix A.1), thereby ensuring that the identified difference to the younger adolescents were beyond the effect of partial voluming.

In vivo derivation of averaged *normalized* cortical myelin maps in the NCANDA adolescent and HCP young adult cohorts revealed higher values in the older than younger group particularly in the striate, motor, occipito-parietal cortices. These regions were marked by high T1-weighted / T2-weighted MRI ratios, indicating heavy myelination. These regions are generally considered unimodal, in that they subserve sensory or motor functions and tend to complete development early. By contrast, multimodal cortex subserves integrative, complex cognitive and emotional functions, which develop later and with continued interaction with the environment (Purger et al. 2016; Snaidero and Simons 2017). Multimodal cortex generally contains lightly myelinated fibers that underlie greater intracortical circuit complexity than unimodal circuitry (Glasser et al. 2014).

4.1 Functional Correlates of Regional Cortical Myelin

The primary function of the frontal motor strip (area 4) is motor control. Evidence for greater lipid content consistent with lateralized, heavy myelination of fibers in area 4 comports with this function. These relations, tested in the NCANDA adolescents, were supported with Pearson correlations and the multiple mediation model indicating a relation between greater *normalized* myelin content in the right hemisphere and faster performance on the Grooved Pegboard Test, especially in the older than younger adolescents when performing in the challenging condition using the non-dominant (typically the left) hand. In apparent contrast to area 4, lower *normalized* myelin content (*i.e.*, relative to the global mean) in the mid or posterior cingulate cortices (areas p24' and 23c) predicted faster grooved

pegboard performance especially by the non-dominant hand. This relation can be explained by recognizing that a function of the cingulate cortex is to support voluntary saccades (Vogt 2016), control over which is critical for eye-hand coordinated movement needed for successful grooved pegboard performance. The complementary relation of unimodal (area 4) and multimodal (areas p24' and 23c) cortices between *normalized* myelin content and function is consistent with the hypothesis that heavy myelination (as in area 4) occurs with simple circuitry (used for speed), whereas lighter myelination occurs with greater intracortical circuit complexity (used for purposefully directed movement). Coordination of such different levels of circuit complexity continues to develop throughout adolescence, and the unimodal/multimodal complementary microstructural changes may represent active synaptic tuning, pruning, and functional development towards an asymptote in young adulthood.

4.2 Validating Adolescent Growth Pattern

Verification of the growth patterns with respect to the NCANDA adolescents, showed that the significance of areas 4, 23c, and p24' were stronger than the impact of the cortical folding in estimating the *normalized* myelin content (see Appendix A.5). Furthermore, the findings were confirmed through a novel longitudinal analysis, which explicitly harmonized the data across visits and was validated using inter- and intra-site human phantom data (see Appendix A.3). Specifically, the significant deceleration of aging effects in the area with significantly greater gains in *normalized* myelin content (i.e., area 4 [R]) and the significant acceleration of aging effects in areas with significantly smaller gains in *normalized* myelin content (i.e., areas 23c [R] and p24' [L]) further supports the hypothesis that development is slowing with early adulthood.

Beyond confirming previous cross-sectional applications of standard T1- and T2-weighted sequences to model cortical myelin development, our longitudinal analysis was novel. This approach resulted in improved reliability of myelin content estimation over multiple visits compared with the cross-sectional approach, i.e., computing myelin content separately for each visit (see Appendix A.3).

4.3 Limitations

Estimating cortical myelin content based on ratio between T1-weighted and T2-weighted MRIs as done in this study could be influenced by iron, which often co-localized with myelin in the cerebral cortex (Fukunaga et al. 2010)). Iron can thus be another contributing factor to MRI contrast showing especially high contrast portions in T2* maps (Stuber et al. 2014). In our analysis, we expect the major fraction of MRI contrast was due to the variation in the myelin content because both the NCANDA and the HCP studies acquired T2-weighted sequences with high sensitivity to lipids. The T2-weighted MRIs also enabled reliable extraction of the brain pial surfaces, and the T1-weighted MRIs were enabled accurate identification of gray/white matter boundaries; together, this image information enhanced accuracy in estimating cortical myelin content on the brain surface. However, not all structural MRI studies share these MRI characteristics and thus must be carefully considered before applying the proposed approach.

Our interpretation of myelin development trajectories was based on the global mean of the raw myelin content, which increased with age before 36 years (Shafee et al. 2015). Around the age of 36, however, myelin density peaks and then declines with advancing adult age (Grydeland et al. 2013). Extending the interpretation of regional development trajectories of the *normalized* myelin content to those later age ranges would thus require more complex modeling.

More complex modelling would also be required when further testing relations between the development of myelin content and neuropsychological functioning. The current analysis focused on correlating *normalized* myelin content to the Grooved Pegboard Test scores of the NCANDA cohort. Measurements capturing more complex neuropsychological functioning, such as derived from resting-state fMRI, have been collected by the HCP and NCANDA study but harmonizing those across studies is generally challenging. When done accurately, one could gain a refined view of the development of cortical myelin and function throughout the brain.

5 Conclusion

Evidence for an extended neurodevelopmental period in humans is useful in posing hypotheses regarding how environmental experiences have the potential for modifying neural circuitry. Experiences can be positive, as in enriching educational situations, or negative, as occurs with psychologically traumatic episodes or initiation of drug or alcohol misuse. Given the continued development of brain circuitry, it is likely that cortical myelination could go awry with untoward events or toxins or be enhanced with enrichment. The findings presented based on tracking of whole-brain, cortical myelin have the potential to guide a mechanistic understanding of normal cortical development. Tracking cortical myelin maturation can also reveal affected regions and microcircuitry underlying cortical neurodevelopmental diseases, such as schizophrenia, which is marked by cortical volume deficits (Ohtani et al. 2014; Selemon 2013; Zipursky et al. 1992), myelin immaturity (Kochunov et al. 2016; Pasternak et al. 2012), and an onset in late adolescence to early adulthood (Keefe and Fenton 2007).

Acknowledgments

Funding. This work was funded by grants from the U.S. National Institute on Alcohol Abuse and Alcoholism: AA021697, AA005965, AA010723, AA017168.

Appendix A:

A.1: Myelin Content with Respect to the Original HCP Data

The Data Release S900 of the Human Connectome Project (HCP) provided for each subject the output of the minimal processing pipeline (Glasser et al. 2013), which included the supratentorial volume and the myelin content scores along the *midthickness* surface (*i.e.*, the surface with equal distance to pial and white matter) based on the raw MRI data (i.e., 0.7mm isotropic resolution). For each voxel inside the cortical gray matter, the pipeline computed a myelin content score by the ratio between T1-weighted and T2-weighted MRI (Glasser and

Van Essen 2011). These voxel-based myelin scores were then mapped to each vertex of the *midthickness* surface by computing their average with respect to a cylinder centered on that vertex. The myelin score at this step is referred to as the *raw* myelin content. To correct for residual bias field of the raw myelin content (Glasser et al. 2013), a 14.14 mm Gaussian filter kernel was applied to the vertex-wise values, the resulting *low frequency patterns* of the myelin content scores were then subtracted from that of the average myelin content across the Conte69 subjects (the *reference* myelin content) (Glasser and Van Essen 2011), and the difference was then added to the vertex-wise values. This score is called the *normalized* myelin content as the myelin distribution is *normalized* to the reference. Finally, the *midthickness* surface encoding the *normalized* myelin content was mapped onto the 2mm HCP template (Glasser et al. 2013), which encoded each hemisphere as a sphere defined by a 2mm standard CIFTI grayordinate space comprising 32k vertices (Glasser et al. 2013).

Figure A.1 **and** A.2 reveal findings that are consistent with respect to the young adults at the lower resolution (see Figure 4 **and** 5). Compared with the lower resolution, myelin content computed with respect to the original resolution generally varied less across age and resulted in significant age-dependent regions that were larger in size. Table A.1 reaffirms the finding that age effects (β_{age}) were less steep for areas 4 ,23c, and p24' compared with those of adolescents (see Table 2). Furthermore, the age effects were bilaterally significant for areas 4 and p24'.

A.2 Correlating Average Regional Normalized Myelin Content and Grooved Pegboard Test Scores

For each region with significant age effects, an *Independent Mediation Model* tested whether the effect of age (independent variable) on the pegboard test scores (dependent variable) was mediated by the average regional *normalized* myelin content (intermediary variable). To measure the indirect effect, the regional and performance scores were first applied to a linear regression model with the confounding factors being sex, svol, site, ethnicity, and handedness (L/R). Separately for each hand, the residual scores and age were applied to the *Independent Mediation Model*. For each effect, the normalized β_N value was computed by dividing the β value of the effect divided with the β value of the direct (unmediated) effect (c_D) between age and the pegboard score. The P-value of an effect was then inferred from Permutation testing (Boca et al. 2014) of the BRAVO toolbox V.2.0 (https://sites.google.com/site/bravotoolbox; iterations: 5000; one-sided t-test) applied to the normalized β_M value. The summary of that analysis is shown in Table A.2.

In the NCANDA group, the relation between age and pegboard scores was most strongly mediated by the myelin content of areas 4 [L], p24' [R] and 4 [R] (where [L] denotes left and [R] denotes right) for both the dominant and non-dominant hand. All three right hemisphere regions showed greater indirect effects for the non-dominant than the dominant hand. Furthermore, the regions associated with significant direct effects of the myelin on the performance scores (Path b_x) agreed with those of the Pearson correlation (Table 3) with the

exception of area 23c[R] on the Dominant hand scores, whose P-value on the intermediate model was right below the significance threshold (P= 0.048).

A.3 Validating Longitudinal Myelin Computation

The longitudinal approach improved the reliability of estimating *normalized* myelin content compared with the cross-sectional approach when applied to the 185 adolescents of the NCANDA data set who participated three times Figure A.3). To verify this finding, the analysis was repeated with respect to travelling human phantoms.

Specifically, the difference in myelin content was measured between scan pairs, where each scan pair consisted of scans of the same subject that were either acquired at both sites (i.e., NCANDA collection site P and O) within 30 days (inter-site scan pair; average number of days between visits was 22.3 days) or acquired at the same site within a day (intra-site scan pair) according to the NCANDA scanning protocol. The data set contained a total of 11 inter-site scan pairs from 3 human phantoms (two women [age 30 and 64], one man [age 41]) and 3 intra-site scan pairs from a single human. The raw myelin content of areas 4, 23c and p24' was computed using the cross-sectional approach (i.e., compute the scores independently for each visit) and the differences in the scores across the scans was computed. The procedure was then repeated for the *normalized* myelin content generated by the cross-sectional and longitudinal approach.

For bihemispheric areas 4, 23c and p24', the longitudinal approach showed lower mean, standard deviation, and maximum differences in the *normalized* myelin content within the inter- and intra-site scan pairs than estimating the *normalized* myelin content independently for each visit (i.e., cross-sectional approach; Figure A.4 and Table A.3). Visual comparison of myelin maps associated with the same human phantom confirmed the previous findings as the *normalized* myelin content across scans was very similar when computed by the longitudinal approach but showed inconsistencies when produced by the cross-sectional approach (see arrows in Figure A.5). The least reliable score was the *raw* myelin content generated by the cross-sectional approach.

A.4 Effects of Normalization

As shown in the Figure A.6, all trajectories of the *normalized* myelin content of the entire cortex and area 4 and p24, had smaller variances than those of the *raw* myelin content, which indicates that much of the between-subject variance in the *raw* myelin content was due to low frequency bias most likely caused by scanner or coil loading variability (Glasser et al. 2013). Furthermore, the plots supported the cortical myelin development hypothesis visualized in Figure 3.

A.5 Effects of Cortical Folding Pattern Removal

To study the effect of cortical folding pattern on our findings, the mean curvature along the cortical surface was regressed out from the *normalized* myelin content of the NCANDA cohort and the analysis for identifying cohort-specific developmental patterns was applied to residual myelin content (Supplemental Figure 7). The entire process was repeated regressing

out convexity instead of curvature. In both experiments, regression had little effect on the findings with the bihemispheric areas 4, 23c and p24', revealing again significant age effects.

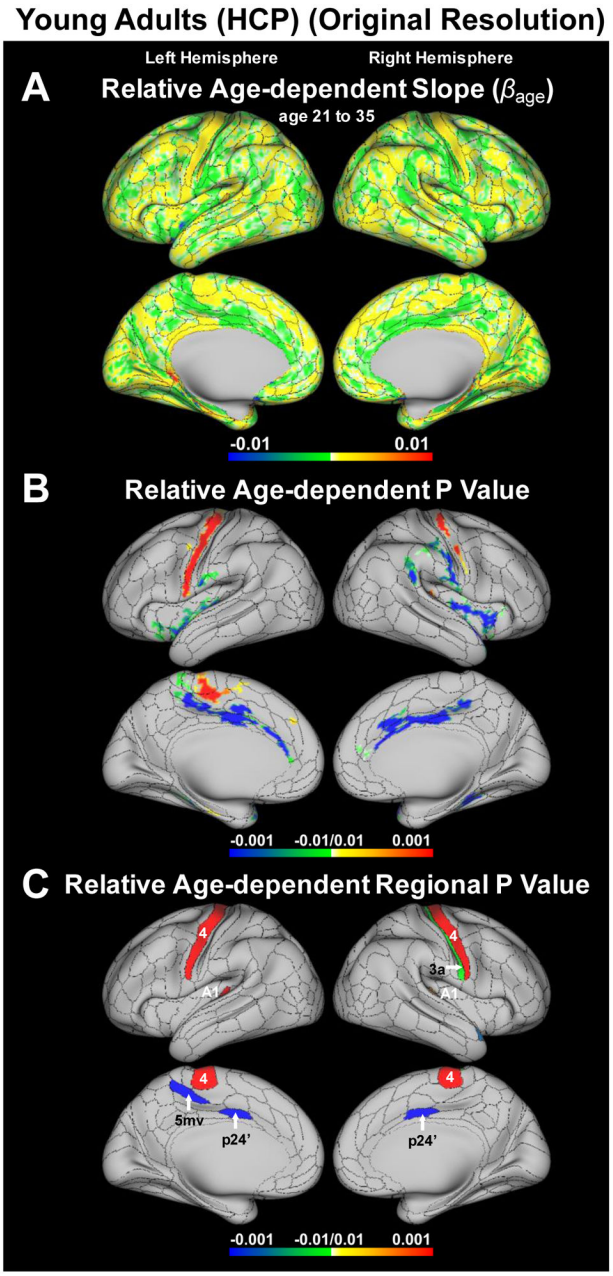

Figure A.1.

Cross-sectional myelin development patterns for young adults (HCP) measured on the original resolution (0.7mm isotropic). (A) Age-related differences are computed from the *normalized* myelin content. The vertex-wise (B) and regional (C) P values of those differences are FWER corrected via permutation testing (iterations: 5000). They are grayed out if non-significant (*i.e.*, $P \geq 0.01$) and have a negative sign if the relative age-effects (β_{age}) were negative, i.e., myelin density showed smaller gains relative to the cortex as a whole.

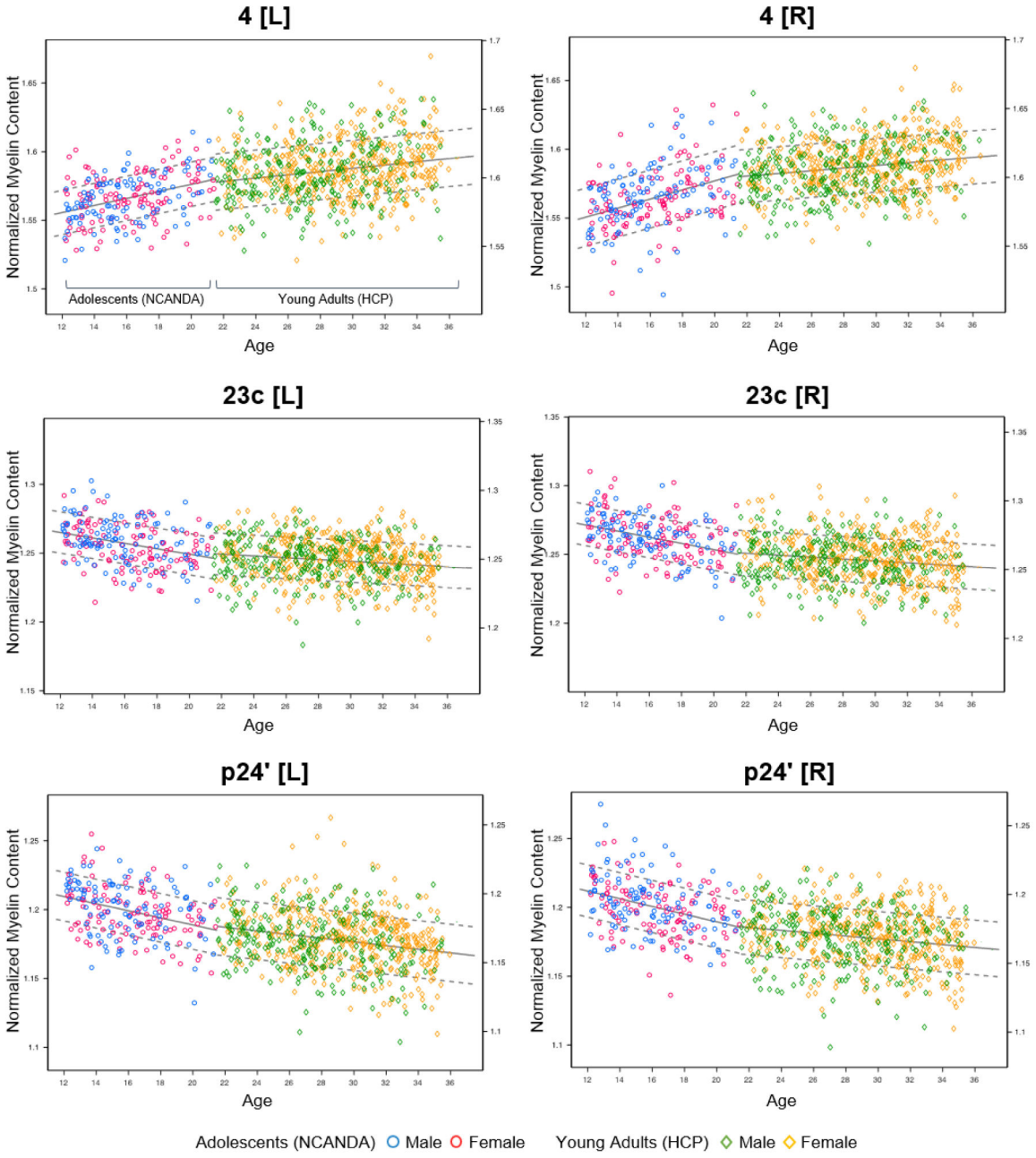

Figure A.2.

Combined cross-sectional normalized myelin development plots of adolescents (NCANDA) based on the original MRIs of NCANDA (resolution: 0.9375×0.9375×1.2mm) and young adults (HCP) based on original MRIS of the HCP (resolution: 0.7mm isotropic). Plots of the *normalized* myelin content for areas 4, 23c, and p24' are shown for left [L] and right [R] hemispheres. In each plot, blue circles represent male and red represent female adolescents; green diamonds represent male and yellow represent female young adults; and the fits of the general liner model +/− SD (standard deviation) are displayed in gray lines. The horizontal axes represent age in years and the vertical axes represent the myelin content (left for adolescents, and right for young adults). Left vertical axis is *normalized* myelin content for

adolescents, and the right is for young adults. The offset of the vertical axis for young adults is adjusted to match with adolescents while the scale is the same. The age of the HCP samples was perturbed by a random number generator (range: [−0.5 0.5]) to improve visualization.

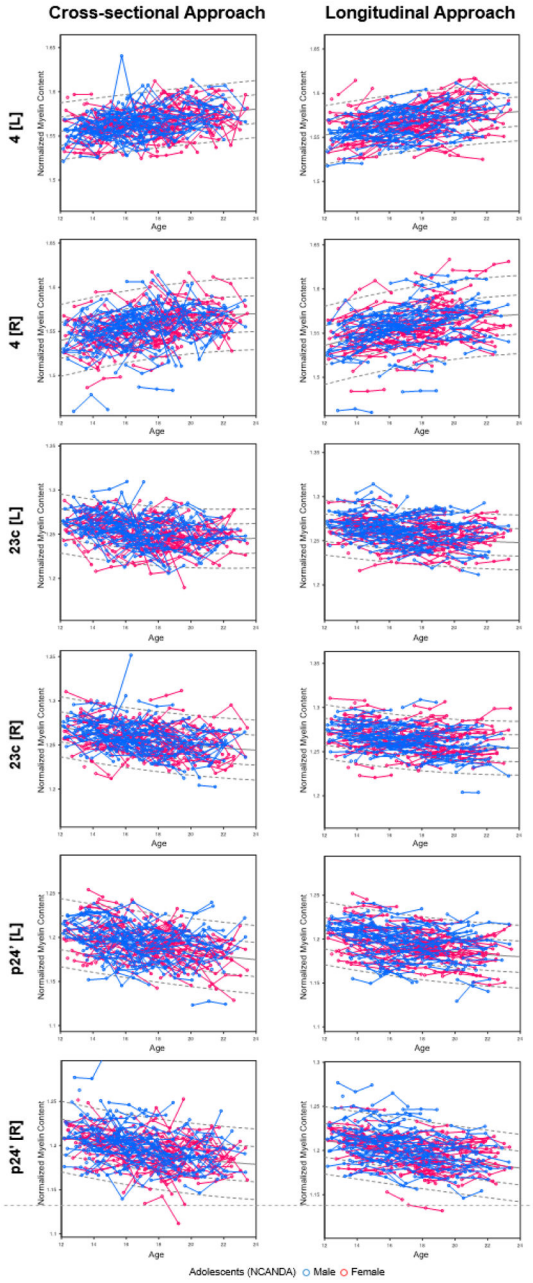

Figure A.3.

Longitudinal plots of myelin scores for adolescents (NCANDA) generated by cross-sectional and longitudinal approaches. Plots of areas 4, 23c, and p24' are shown for the cross-sectional approach (left column) and the longitudinal approach (right column). In each plot, blue circles stand for male and red for female adolescents; visits are connected for each subject. The fits of the linear mixed effects model are drawn in gray with +/− 1 and 2 SD. The horizontal axes represent age (in years) and vertical axes represent the *normalized* myelin content.

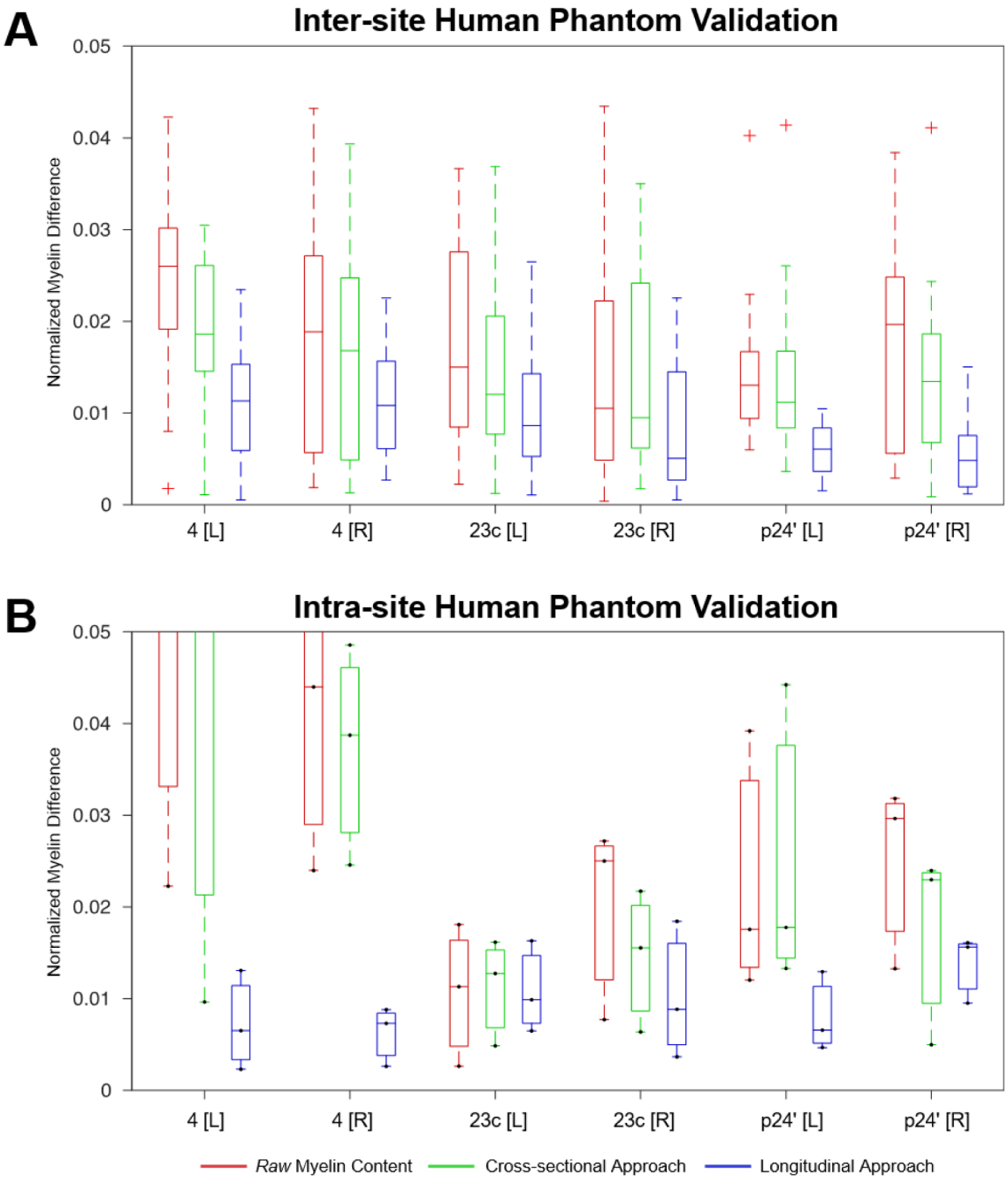

Figure A.4.

Boxplots for intra-site and inter-site human phantom validations. The inter-site validation shown in (A) measured differences of myelin content between scan pairs (total 11 pairs from 3 human phantoms used) collected one at each NCANDA site (sites P and O) within 30 days. The intra-site validation shown in (B) measured differences of myelin content between scan and same day rescan pairs (total 3 pairs from a human phantom used) at NCANDA sites. For (A) and (B), cross-sectional approach using the *raw* myelin content (red), cross-sectional approach using the *normalized* myelin content (green) and the longitudinal approach using the *normalized* myelin content (blue) are compared for bihemispheric areas

4, 23c and p24'. Each boxplot shows the median, 25th and 75th percentiles. The whiskers extend to the most extreme data points except for outliers, which are plotted as '+'. In (B), individual data points are shown as black dots.

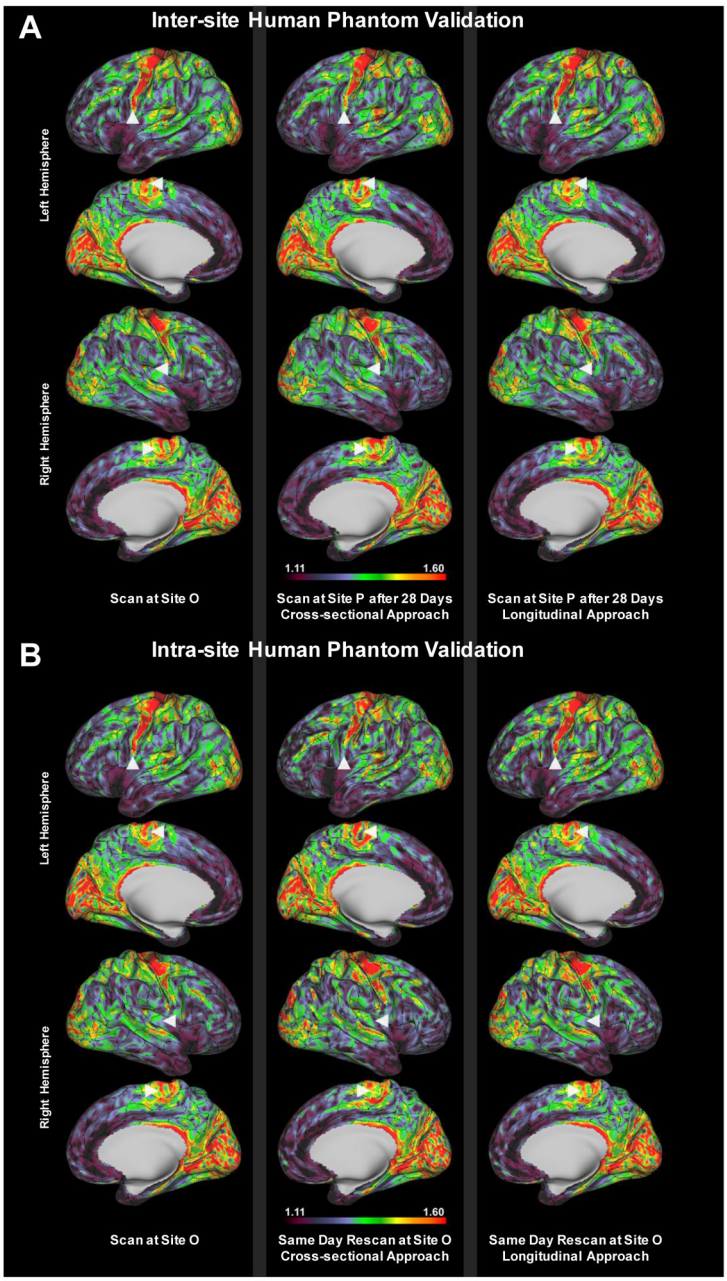

Figure A.5.

Single human phantom examples for intra-site and inter-site human phantom validations. For both (A) inter- and (B) intra-site validations, the *normalized* myelin content for the first scan is shown in the left column, the middle column shows the myelin content for the second scan estimated by cross-sectional approach, and in the right column by the longitudinal approach, respectively. Arrowheads point to regions showing visually noticeable differences. The range of color bar is the same across all figures.

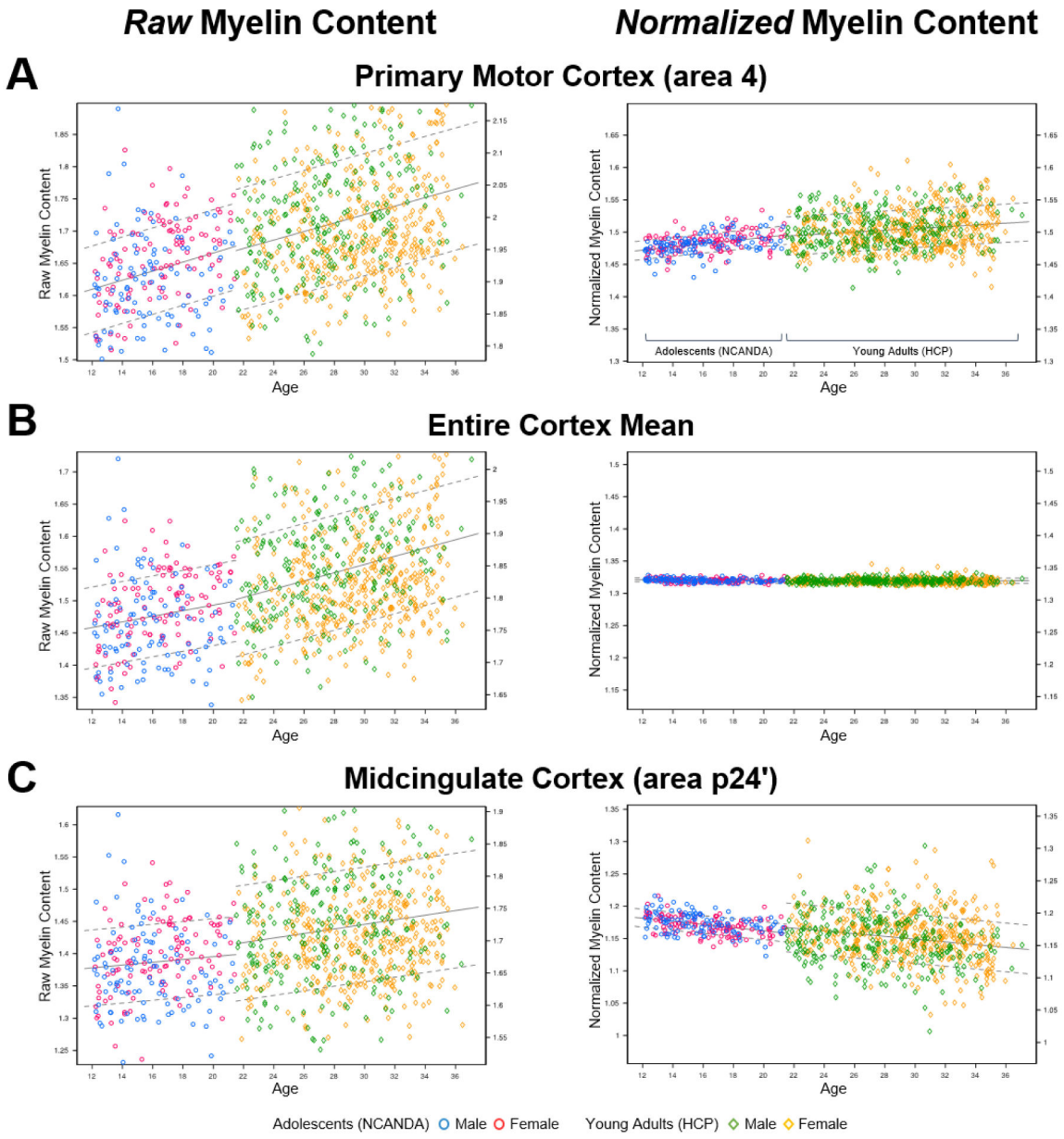

Figure A.6.

Observations from adolescents (NCANDA) and young adults (HCP) data for the cortical myelin development hypothesis. For each *raw* (left column) and *normalized* (right column) myelin content, example observations for (A) primary motor cortex (bihemispheric mean of area 4), (B) mean over the entire cortex, and (C) midcingulate cortex (bihemispheric mean of area p24') are displayed. In each plot, blue circles represent male and red represent female adolescents; green diamonds represent male and yellow represent female young adults; and the fits of the general liner model with +/− SD (standard deviation) are displayed in gray lines. The horizontal axes represent age in years and the vertical axes represent the myelin content (left for adolescents, and right for young adults). The offset of the vertical axis for young adults is adjusted to match with adolescents while the scale is the same. The age of

the HCP samples was perturbed by a random number generator (range: [−0.5 0.5]) to improve visualization. Between left (the *raw* myelin content) and right (the *normalized* myelin content) columns, the same axis scale was used for comparisons.

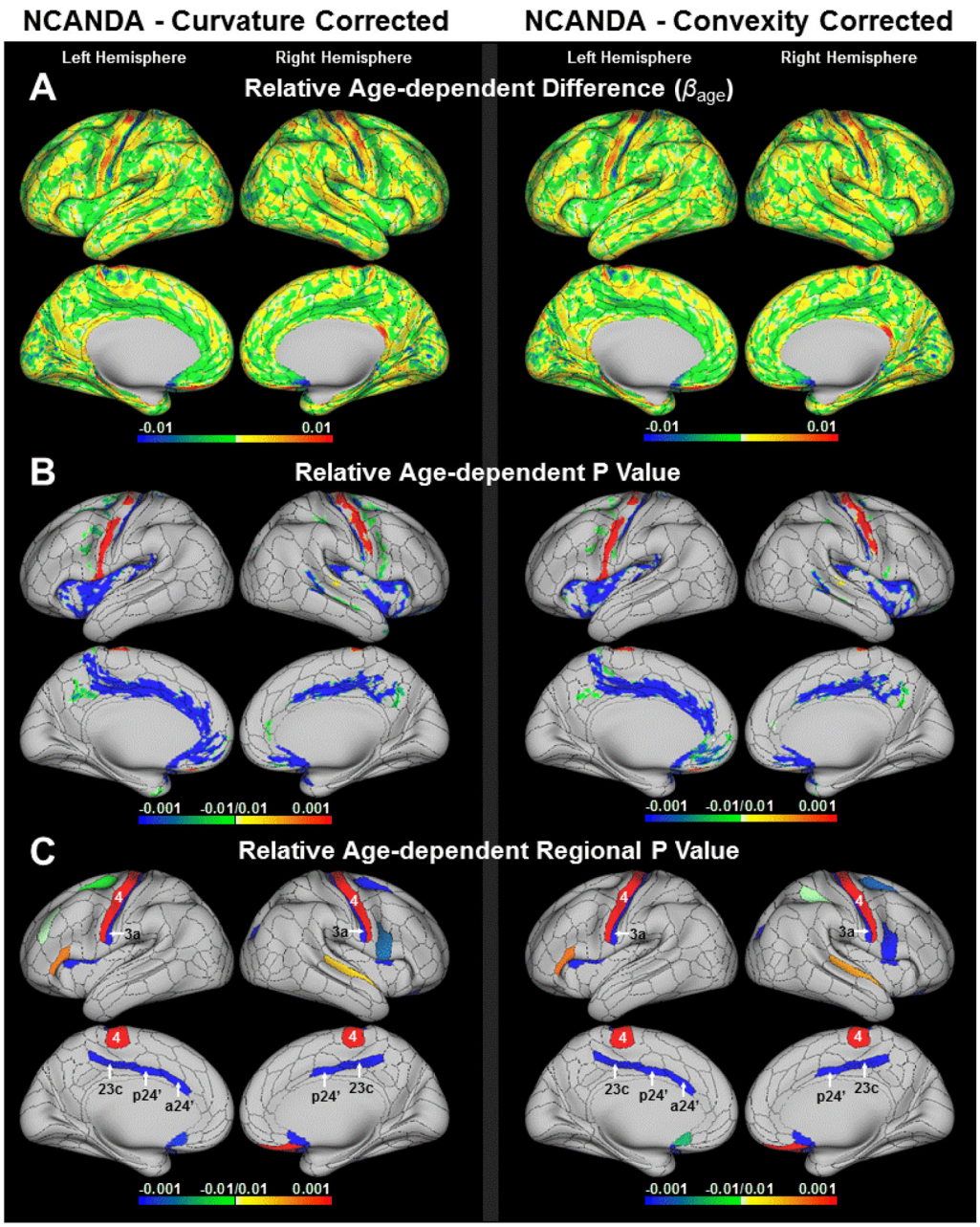

Figure A.7.

Cross-sectional myelin development patterns for adolescents (NCANDA) after curvature or convexity (sulc) corrected. (A) Age-related differences are computed from the normalized myelin content (i.e., the change in myelin content relative to the mean over the entire cortex) by applying a general linear model that views age as a predictor and sex, ethnicity, svol as confounding factors. Each value is displayed on the averaged (inflated) brain surface of the corresponding cohort with the boundaries of the HCP multimodal parcellation atlas (MMP 1.0) overlaid. The vertex-wise (B) and regional (C) P values of those differences are FWER corrected via permutation testing (iterations: 5000). They are grayed out if non-significant

(i.e., P ≥ 0.01) and have a negative sign if the relative age-effects (β_{age}) were negative, i.e., myelin density showed smaller gains relative to the entire cortex.

Table A.1.

Cross-sectional age effects with respect to the *normalized* myelin content for young adults (HCP) estimated on the original resolution (0.7mm isotropic)

ROI	Hemi	HCP Baseline	
		β_{age}	P
4	L	0.0012	< **0.001**
4	R	0.0010	< **0.001**
23c	L	−0.0006	0.016
23c	R	−0.0007	0.018
p24'	L	−0.0013	< **0.001**
p24'	R	−0.0010	< **0.001**

P values are marked bold if P < 0.01.

Table A.2.

Individual Mediation tests for age, average *normalized* myelin content, and Grooved Pegboard Test scores for NCANDA adolescents

ROI	Hemi	Path a_x		Path b_x		Path c_M (direct effect)			Path $a_x b_x$ (indirect effect)		
		β_a	P	β_b	P	β_c	P	β_N	$\beta_a \cdot \beta_b$	P	β_N
Dominant Hand											
Path d (total effect, Unmediated Model): β_d = −1.283, P < 0.001											
4	L	0.005	< **0.001**	−87.83	**0.002**	−0.848	**0.003**	66%	−0.435	< **0.001**	34%
4	R	0.005	< **0.001**	−40.72	0.062	−1.086	< **0.001**	85%	−0.197	< **0.001**	15%
23c	L	−0.003	< **0.001**	23.86	0.300	−1.223	< **0.001**	95%	−0.061	0.019	5%
23c	R	−0.002	< **0.001**	73.60	**0.048**	−1.114	< **0.001**	87%	−0.169	< **0.001**	13%
p24'	L	−0.003	< **0.001**	−26.19	0.251	−1.353	< **0.001**	105%	0.070	**0.009**	−5%
p24'	R	−0.003	< **0.001**	84.89	**0.010**	−1.051	< **0.001**	82%	−0.232	< **0.001**	18%
Non-Dominant Hand											
Path d (total effect, Unmediated Model): β_d = −1.387, P < 0.001											
4	L	0.005	< **0.001**	−92.80	**0.005**	−0.927	**0.002**	67%	−0.459	< **0.001**	33%
4	R	0.005	< **0.001**	−68.98	**0.011**	−1.053	< **0.001**	76%	−0.334	< **0.001**	24%
23c	L	−0.003	< **0.001**	121.11	**0.008**	−1.080	< **0.001**	78%	−0.307	< **0.001**	22%
23c	R	−0.002	< **0.001**	97.43	**0.024**	−1.164	< **0.001**	84%	−0.223	< **0.001**	16%
p24'	L	−0.003	< **0.001**	−37.79	0.200	−1.488	< **0.001**	107%	0.101	**0.002**	−7%
p24'	R	−0.003	< **0.001**	129.52	**0.001**	−1.033	**0.002**	74%	−0.354	< **0.001**	25%

P < 0.05 are marked bold; in most cases, P < 0.001. The Grooved Pegboard Test score is the total time in seconds to complete the test; shorter time indicates better performance. The normalized β_N value is the ratio between β value of an effect according to the mediation model divided by β_d, the β value of the direct (unmediated) effect between age and the pegboard score.

Table A.3

Statistics of myelin content differences for inter- and Inter-site human phantom validations

Inter-site Human Phantom Validation										
		***Raw* Myelin Content**			**Cross-sectional Approach**			**Longitudinal Approach**		
ROI	**Hemi**	**Mean**	**SD**	**Max**	**Mean**	**SD**	**Max**	**Mean**	**SD**	**Max**
4	L	0.024	0.011	0.042	0.019	0.009	0.030	**0.011**	**0.006**	**0.023**
4	R	0.020	0.017	0.064	0.017	0.015	0.054	**0.011**	**0.008**	**0.026**
23c	L	0.015	0.009	0.040	0.015	0.010	0.041	**0.006**	**0.003**	**0.010**
23c	R	0.018	0.013	0.043	0.016	0.012	0.039	**0.011**	**0.006**	**0.023**
p24'	L	0.015	0.013	0.043	0.016	0.011	0.035	**0.008**	**0.007**	**0.023**
p24'	R	0.018	0.011	0.038	0.015	0.011	0.041	**0.005**	**0.004**	**0.015**

Inter-site Human Phantom Validation										
		***Raw* Myelin Content**			**Cross-sectional Approach**			**Longitudinal Approach**		
ROI	**Hemi**	**Mean**	**SD**	**Max**	**Mean**	**SD**	**Max**	**Mean**	**SD**	**Max**
4	L	0.052	0.021	0.068	0.043	0.024	0.064	**0.007**	**0.004**	**0.013**
4	R	**0.011**	0.006	0.018	**0.011**	0.005	**0.016**	**0.011**	**0.004**	**0.016**
23c	L	0.023	0.012	0.039	0.025	0.014	0.044	**0.008**	**0.004**	**0.013**
23c	R	0.043	0.015	0.061	0.037	0.010	0.049	**0.006**	**0.003**	**0.009**
p24'	L	0.020	0.009	0.027	0.015	**0.006**	0.022	**0.010**	**0.006**	**0.018**
p24'	R	0.025	0.008	0.032	0.017	0.009	0.024	**0.014**	**0.003**	**0.016**

Mean, SD or Max values are marked bold if performed best among approaches.

References

American Psychiatric Association (2000), Diagnostic and statistical manual of mental disorders : DSM-IV-TR (4th edn.; Washington, DC: American Psychiatric Association) xxxvii, 943 p.

Arshad M, Stanley JA, and Raz N (2017), 'Test-retest reliability and concurrent validity of in vivo myelin content indices: Myelin water fraction and calibrated T1 w/T2 w image ratio', Hum Brain Mapp, 38 (4), 1780–90. [PubMed: 28009069]

Avants BB, et al. (2008), 'Symmetric diffeomorphic image registration with cross-correlation: evaluating automated labeling of elderly and neurodegenerative brain', Med Image Anal, 12 (1), 26–41. [PubMed: 17659998]

Bava S and Tapert SF (2010), 'Adolescent brain development and the risk for alcohol and other drug problems', Neuropsychol Rev, 20 (4), 398–413. [PubMed: 20953990]

Bernal-Rusiel JL, et al. (2013), 'Statistical analysis of longitudinal neuroimage data with Linear Mixed Effects models', Neuroimage, 66, 249–60. [PubMed: 23123680]

Boca SM, et al. (2014), 'Testing multiple biological mediators simultaneously', Bioinformatics, 30 (2), 214–20. [PubMed: 24202540]

Bock NA, et al. (2009), 'Visualizing the entire cortical myelination pattern in marmosets with magnetic resonance imaging', J Neurosci Methods, 185 (1), 15–22. [PubMed: 19737577]

Bock NA, et al. (2013), 'Optimizing T1-weighted imaging of cortical myelin content at 3.0 T', Neuroimage, 65, 1–12. [PubMed: 23036446]

Brown SA, et al. (2015), 'The National Consortium on Alcohol and NeuroDevelopment in Adolescence (NCANDA): A Multisite Study of Adolescent Development and Substance Use', J Stud Alcohol Drugs, 76 (6), 895–908. [PubMed: 26562597]

Casey BJ, Giedd JN, and Thomas KM (2000), 'Structural and functional brain development and its relation to cognitive development', Biol Psychol, 54 (1–3), 241–57. [PubMed: 11035225]

Coupe P, et al. (2008), 'An optimized blockwise nonlocal means denoising filter for 3-D magnetic resonance images', IEEE Trans Med Imaging, 27 (4), 425–41. [PubMed: 18390341]

Cox RW (1996), 'AFNI: software for analysis and visualization of functional magnetic resonance neuroimages', Comput Biomed Res, 29 (3), 162–73. [PubMed: 8812068]

Dale AM, Fischl B, and Sereno MI (1999), 'Cortical surface-based analysis. I. Segmentation and surface reconstruction', Neuroimage, 9 (2), 179–94. [PubMed: 9931268]

Fischl B (2012), 'FreeSurfer', Neuroimage, 62 (2), 774–81. [PubMed: 22248573]

Fischl B, Sereno MI, and Dale AM (1999), 'Cortical surface-based analysis. II: Inflation, flattening, and a surface-based coordinate system', Neuroimage, 9 (2), 195–207. [PubMed: 9931269]

Fischl B, et al. (2004), 'Sequence-independent segmentation of magnetic resonance images', Neuroimage, 23 Suppl 1, S69–84. [PubMed: 15501102]

Fjell AM, et al. (2012), 'Multimodal imaging of the self-regulating developing brain', Proc Natl Acad Sci U S A, 109 (48), 19620–5. [PubMed: 23150548]

Fukunaga M, et al. (2010), 'Layer-specific variation of iron content in cerebral cortex as a source of MRI contrast', Proc Natl Acad Sci U S A, 107 (8), 3834–9. [PubMed: 20133720]

Ganzetti M, Wenderoth N, and Mantini D (2014), 'Whole brain myelin mapping using T1- and T2-weighted MR imaging data', Front Hum Neurosci, 8, 671. [PubMed: 25228871]

Giedd JN, et al. (2015), 'Child psychiatry branch of the National Institute of Mental Health longitudinal structural magnetic resonance imaging study of human brain development', Neuropsychopharmacology, 40 (1), 43–9. [PubMed: 25195638]

Glasser MF and Van Essen DC (2011), 'Mapping human cortical areas in vivo based on myelin content as revealed by T1- and T2-weighted MRI', J Neurosci, 31 (32), 11597–616. [PubMed: 21832190]

Glasser MF, et al. (2014), 'Trends and properties of human cerebral cortex: correlations with cortical myelin content', Neuroimage, 93 Pt 2, 165–75. [PubMed: 23567887]

Glasser MF, et al. (2016), 'A multi-modal parcellation of human cerebral cortex', Nature, 536 (7615), 171–8. [PubMed: 27437579]

Glasser MF, et al. (2013), 'The minimal preprocessing pipelines for the Human Connectome Project', Neuroimage, 80, 105–24. [PubMed: 23668970]

Grydeland H, et al. (2016), 'Intracortical Posterior Cingulate Myelin Content Relates to Error Processing: Results from T1- and T2-Weighted MRI Myelin Mapping and Electrophysiology in Healthy Adults', Cereb Cortex, 26 (6), 2402–10. [PubMed: 25840423]

Grydeland H, et al. (2013), 'Intracortical myelin links with performance variability across the human lifespan: results from T1- and T2-weighted MRI myelin mapping and diffusion tensor imaging', J Neurosci, 33 (47), 18618–30. [PubMed: 24259583]

Iglesias JE, et al. (2011), 'Robust brain extraction across datasets and comparison with publicly available methods', IEEE Trans Med Imaging, 30 (9), 1617–34. [PubMed: 21880566]

Jernigan TL, et al. (1991), 'Maturation of human cerebrum observed in vivo during adolescence', Brain, 114 (Pt 5), 2037–49. [PubMed: 1933232]

Keefe RS and Fenton WS (2007), 'How should DSM-V criteria for schizophrenia include cognitive impairment?', Schizophr Bull, 33 (4), 912–20. [PubMed: 17567627]

Kochunov P, et al. (2016), 'Heterochronicity of white matter development and aging explains regional patient control differences in schizophrenia', Hum Brain Mapp, 37 (12), 4673–88. [PubMed: 27477775]

Lafayette-Instrument (2002), 'Grooved Pegboard Test User Instructions (Model32025)', (Rel. 9.2.03: Lafayette Instrument).

Leuze C, et al. (2017), 'The separate effects of lipids and proteins on brain MRI contrast revealed through tissue clearing', Neuroimage, 156, 412–22. [PubMed: 28411157]

Lutti A, et al. (2014), 'Using high-resolution quantitative mapping of R1 as an index of cortical myelination', Neuroimage, 93 Pt 2, 176–88. [PubMed: 23756203]

MacKay A, et al. (1994), 'In vivo visualization of myelin water in brain by magnetic resonance', Magn Reson Med, 31 (6), 673–7. [PubMed: 8057820]

Miller DJ, et al. (2012), 'Prolonged myelination in human neocortical evolution', Proc Natl Acad Sci U S A, 109 (41), 16480–5. [PubMed: 23012402]

Muller-Oehring EM, et al. (2017), 'Influences of Age, Sex, and Moderate Alcohol Drinking on the Intrinsic Functional Architecture of Adolescent Brains', Cereb Cortex, 1–15. [PubMed: 28365777]

Nichols BN and Pohl KM (2015), 'Neuroinformatics Software Applications Supporting Electronic Data Capture, Management, and Sharing for the Neuroimaging Community', Neuropsychol Rev, 25 (3), 356–68. [PubMed: 26267019]

Nieuwenhuys R (2013), 'The myeloarchitectonic studies on the human cerebral cortex of the Vogt-Vogt school, and their significance for the interpretation of functional neuroimaging data', Brain Struct Funct, 218 (2), 303–52. [PubMed: 23076375]

Ohtani T, et al. (2014), 'Prefrontal cortex volume deficit in schizophrenia: a new look using 3T MRI with manual parcellation', Schizophr Res, 152 (1), 184–90. [PubMed: 24280350]

Oldfield RC (1971), 'The assessment and analysis of handedness: the Edinburgh inventory', Neuropsychologia, 9 (1), 97–113. [PubMed: 5146491]

Pasternak O, et al. (2012), 'Excessive extracellular volume reveals a neurodegenerative pattern in schizophrenia onset', J Neurosci, 32 (48), 17365–72. [PubMed: 23197727]

Pfefferbaum A, et al. (2016), 'Adolescent Development of Cortical and White Matter Structure in the NCANDA Sample: Role of Sex, Ethnicity, Puberty, and Alcohol Drinking', Cereb Cortex, 26 (10), 4101–21. [PubMed: 26408800]

Pohl KM, et al. (2016), 'Harmonizing DTI measurements across scanners to examine the development of white matter microstructure in 803 adolescents of the NCANDA study', Neuroimage, 130, 194–213. [PubMed: 26872408]

Purger D, Gibson EM, and Monje M (2016), 'Myelin plasticity in the central nervous system', Neuropharmacology, 110 (Pt B), 563–73. [PubMed: 26282119]

Raznahan A, et al. (2012), 'Prenatal growth in humans and postnatal brain maturation into late adolescence', Proc Natl Acad Sci U S A, 109 (28), 11366–71. [PubMed: 22689983]

Robinson EC, et al. (2014), 'MSM: a new flexible framework for Multimodal Surface Matching', Neuroimage, 100, 414–26. [PubMed: 24939340]

Rohlfing T and Maurer CR Jr. (2003), 'Nonrigid image registration in shared-memory multiprocessor environments with application to brains, breasts, and bees', IEEE Trans Inf Technol Biomed, 7 (1), 16–25. [PubMed: 12670015]

Rohlfing T, Russakoff DB, and Maurer CR Jr. (2004), 'Performance-based classifier combination in atlas-based image segmentation using expectation-maximization parameter estimation', IEEE Trans Med Imaging, 23 (8), 983–94. [PubMed: 15338732]

Rohlfing T, et al. (2014), 'N-CANDA data integration: anatomy of an asynchronous infrastructure for multi-site, multi-instrument longitudinal data capture', J Am Med Inform Assoc, 21 (4), 758–62. [PubMed: 24296908]

Rowley CD, et al. (2017), 'Age-related mapping of intracortical myelin from late adolescence to middle adulthood using T1 -weighted MRI', Hum Brain Mapp.

Sadananthan SA, et al. (2010), 'Skull stripping using graph cuts', Neuroimage, 49 (1), 225–39. [PubMed: 19732839]

Selemon LD (2013), 'A role for synaptic plasticity in the adolescent development of executive function', Transl Psychiatry, 3, e238. [PubMed: 23462989]

Shafee R, Buckner RL, and Fischl B (2015), 'Gray matter myelination of 1555 human brains using partial volume corrected MRI images', Neuroimage, 105, 473–85. [PubMed: 25449739]

Shaw P, et al. (2008), Neurodevelopmental trajectories of the human cerebral cortex', J Neurosci, 28 (14), 3586–94. [PubMed: 18385317]

Sigalovsky IS, Fischl B, and Melcher JR (2006), 'Mapping an intrinsic MR property of gray matter in auditory cortex of living humans: a possible marker for primary cortex and hemispheric differences', Neuroimage, 32 (4), 1524–37. [PubMed: 16806989]

Sled JG, Zijdenbos AP, and Evans AC (1998), 'A nonparametric method for automatic correction of intensity nonuniformity in MRI data', IEEE Trans Med Imaging, 17 (1), 87–97. [PubMed: 9617910]

Smith SM (2002), 'Fast robust automated brain extraction', Hum Brain Mapp, 17 (3), 143–55. [PubMed: 12391568]

Snaidero N and Simons M (2017), 'The logistics of myelin biogenesis in the central nervous system', Glia, 65 (7), 1021–31. [PubMed: 28168748]

Sowell ER, et al. (2003), 'Mapping cortical change across the human life span', Nat Neurosci, 6 (3), 309–15. [PubMed: 12548289]

Squeglia LM, et al. (2015), 'Brain development in heavy-drinking adolescents', Am J Psychiatry, 172 (6), 531–42. [PubMed: 25982660]

Stiles J and Jernigan TL (2010), 'The basics of brain development', Neuropsychol Rev, 20 (4), 327–48. [PubMed: 21042938]

Stuber C, et al. (2014), 'Myelin and iron concentration in the human brain: a quantitative study of MRI contrast', Neuroimage, 93 Pt 1, 95–106. [PubMed: 24607447]

Sullivan EV, et al. (2016), 'Cognitive, emotion control, and motor performance of adolescents in the NCANDA study: Contributions from alcohol consumption, age, sex, ethnicity, and family history of addiction', Neuropsychology, 30 (4), 449–73. [PubMed: 26752122]

Tomassy GS, Dershowitz LB, and Arlotta P (2016), 'Diversity Matters: A Revised Guide to Myelination', Trends Cell Biol, 26 (2), 135–47. [PubMed: 26442841]

Tustison NJ, et al. (2010), 'N4ITK: improved N3 bias correction', IEEE Trans Med Imaging, 29 (6), 1310–20. [PubMed: 20378467]

Van Essen DC, et al. (2013), 'The WU-Minn Human Connectome Project: an overview', Neuroimage, 80, 62–79. [PubMed: 23684880]

Vogt BA (2016), 'Midcingulate cortex: Structure, connections, homologies, functions and diseases', J Chem Neuroanat, 74, 28–46. [PubMed: 26993424]

Vogt BA, et al. (1995), 'Human cingulate cortex: surface features, flat maps, and cytoarchitecture', J Comp Neurol, 359 (3), 490–506. [PubMed: 7499543]

Whittall KP, et al. (1997), 'In vivo measurement of T2 distributions and water contents in normal human brain', Magn ResonMed, 37 (1), 34–43.

Winkler AM, et al. (2014), 'Permutation inference for the general linear model', Neuroimage, 92, 381–97. [PubMed: 24530839]

Yoshiura T, et al. (2000), 'Heschl and superior temporal gyri: low signal intensity of the cortex on T2-weighted MR images of the normal brain', Radiology, 214 (1), 217–21. [PubMed: 10644127]

Zipursky RB, et al. (1992), 'Widespread cerebral gray matter volume deficits in schizophrenia', Archives of General Psychiatry, 49, 195–205. [PubMed: 1567274]

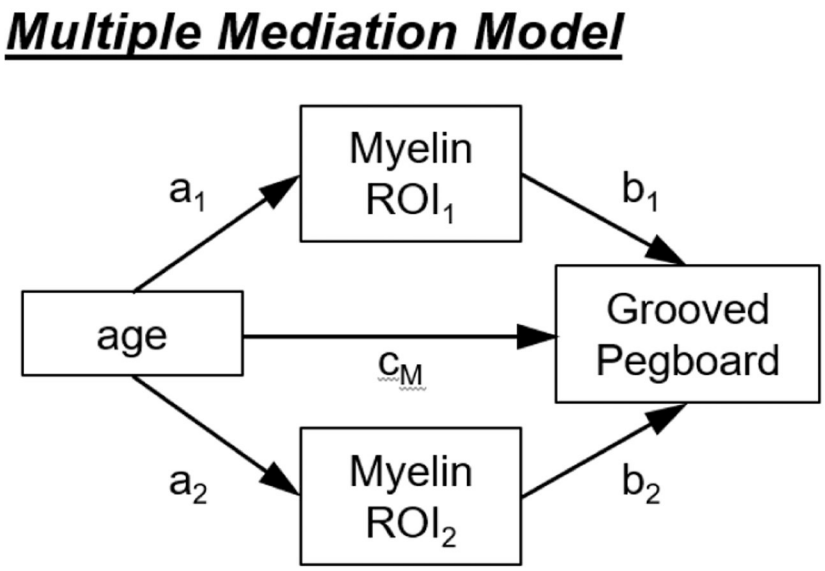

Figure 1.

The *Multiple Mediation Model* examined which of two regional myelin scores had a significantly stronger indirect effect (i.e., accounted for greater variance) on the correlation c_M between age and the Grooved Pegboard Test scores (total time in seconds). Path c_M represents the direct effect and the paths a_1b_1, and a_2b_2 reflect the indirect effects. The model was applied separately with respect to the dominant and non-dominant hand.

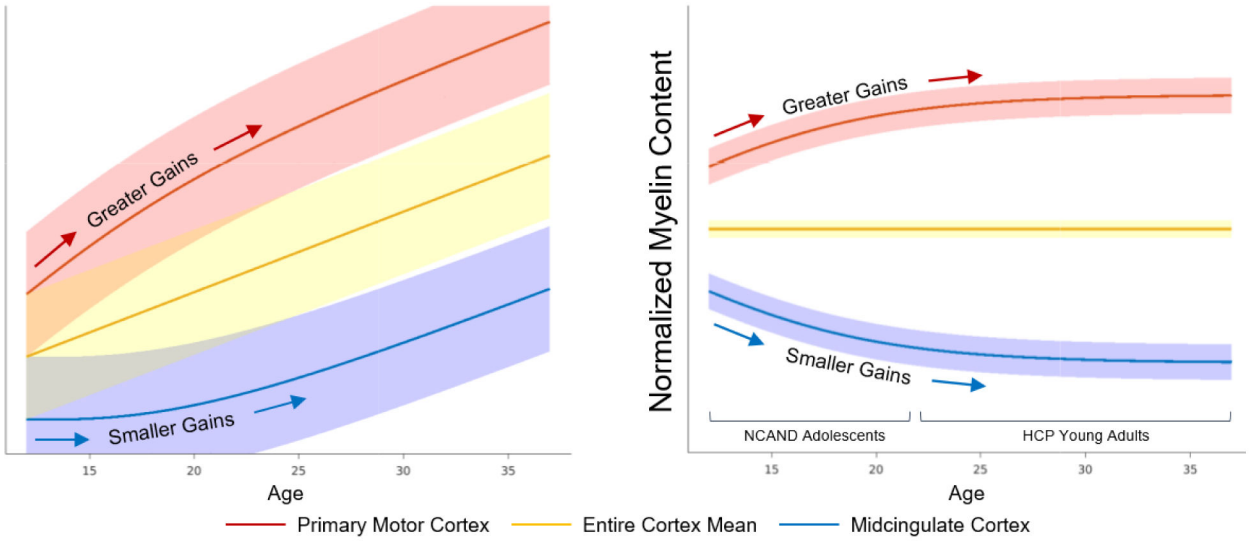

Figure 2.

Cortical myelin development hypothesis for NCANDA adolescents and HCP young adults. The developmental trajectories of the *raw* (left) and the *normalized* (right) myelin content are displayed for primary motor cortex (red), mean over the entire cortex (yellow) and midcingulate cortex (blue). The predicted variances are shown as shaded error bounds with corresponding colors. Between the *raw* and *normalized* myelin content, the deviation from the mean of the entire cortex is preserved in primary motor and midcingulate cortices. The age-dependent inter- subject variance is now much smaller for the *normalized* myelin content.

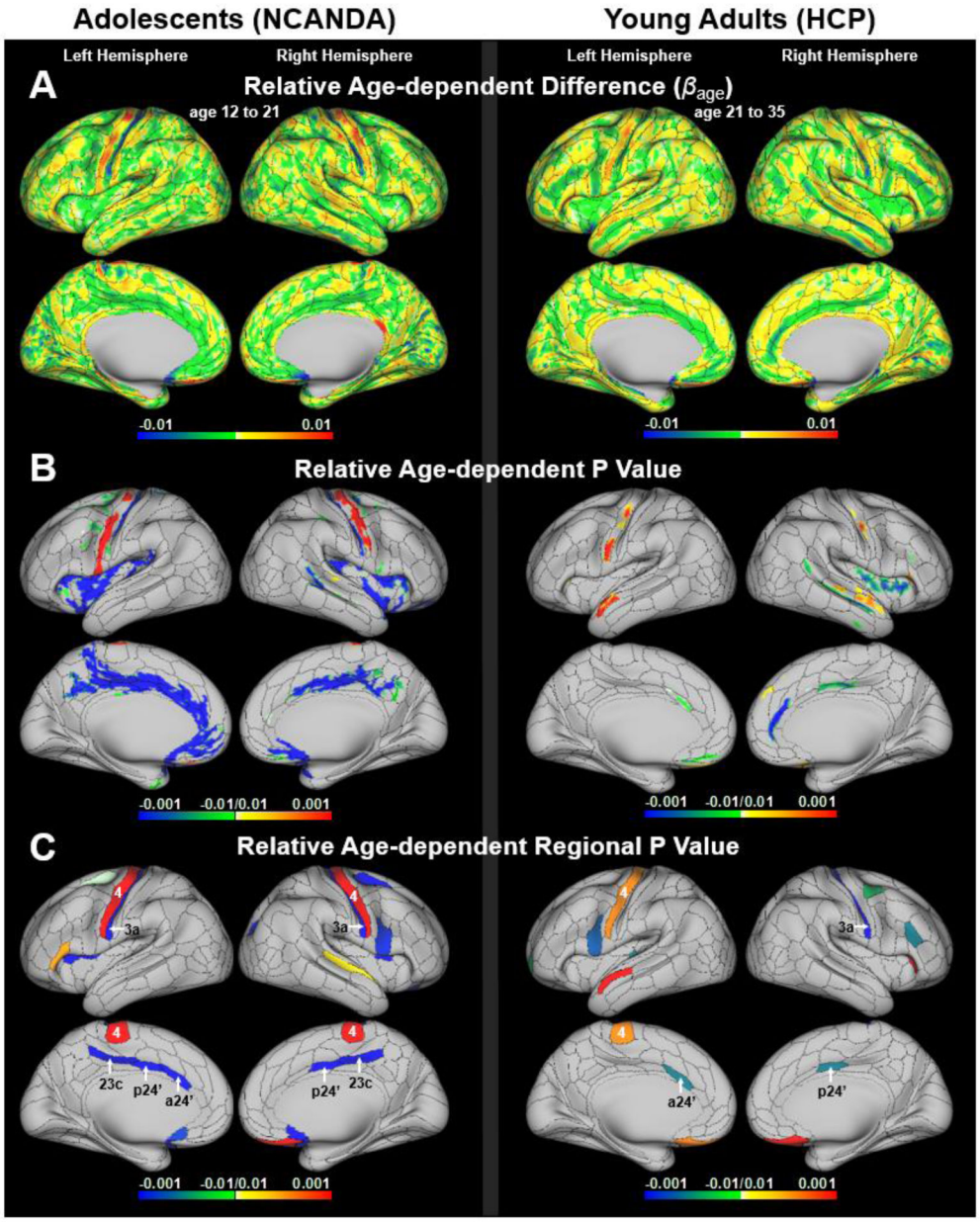

Figure 3.

Cross-sectional myelin development patterns for adolescents (NCANDA) and young adults (HCP). (A) For both cohorts, age-related differences are computed from the *normalized* myelin content (*i.e.*, the change in myelin content relative to the mean over the entire cortex) by applying a general linear model that views age as a predictor and sex, ethnicity, svol, and site (omitted in HCP) as confounding factors. Each value is displayed on the averaged (inflated) brain surface of the corresponding cohort with the boundaries of the HCP multimodal parcellation atlas (MMP 1.0) overlaid. The vertex-wise (B) and regional (C) P values of those slopes are FWER corrected via permutation testing (iterations: 5000). They are grayed out if non-significant (*i.e.*, $P \geq 0.01$), have a negative sign (i.e., $\beta_{age} < 0$) if the

gain in myelin density with respect to age was smaller and positive (i.e., $\beta_{age} > 0$) if the gain was larger than the entire cortex.

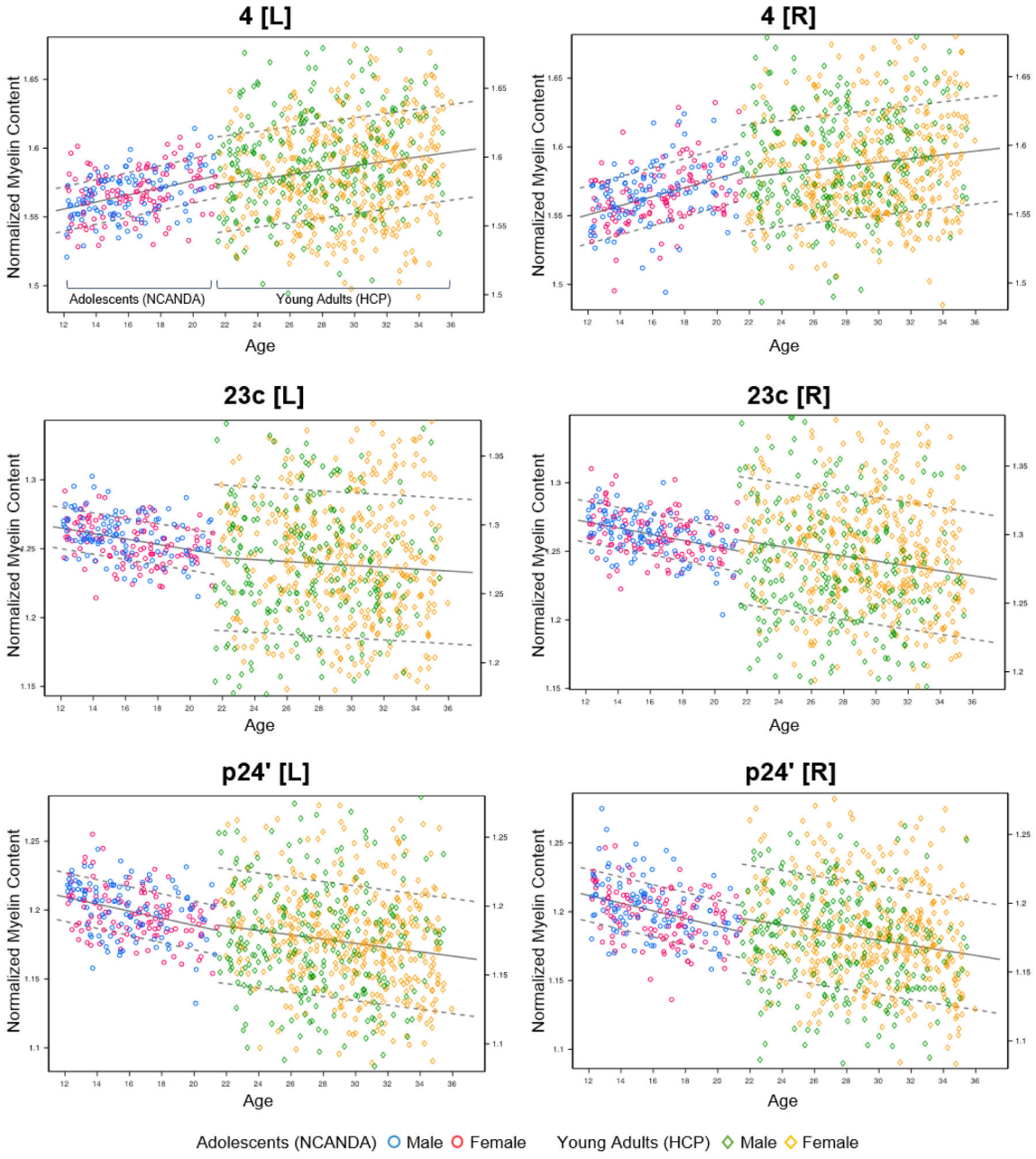

Figure 4.

Combined cross-sectional myelin development plots of adolescents (NCANDA) and young adults (HCP). Plots of the *normalized* myelin content for areas 4, 23c, and p24' are shown for left [L] and right [R] hemispheres. In each plot, blue circles represent male and red represent female adolescents; green diamonds represent male and yellow represent female young adults; and the fits of the general liner model +/− SD (standard deviation) are displayed in gray lines. The horizontal axes represent age in years and the vertical axes represent the myelin content (left for adolescents, and right for young adults). Left vertical axis is *normalized* myelin content for adolescents, and the right is for young adults. **To improve visualization,** the offset of the vertical axis for young adults is adjusted to match

with adolescents while the scale is the same. **Furthermore,** the age of the HCP samples was perturbed by a random number generator (range: [−0.5 0.5]). **Note, the regression is separately performed for each data set so that neither adjusting the offset nor perturbing the age would result in significantly different findings**.

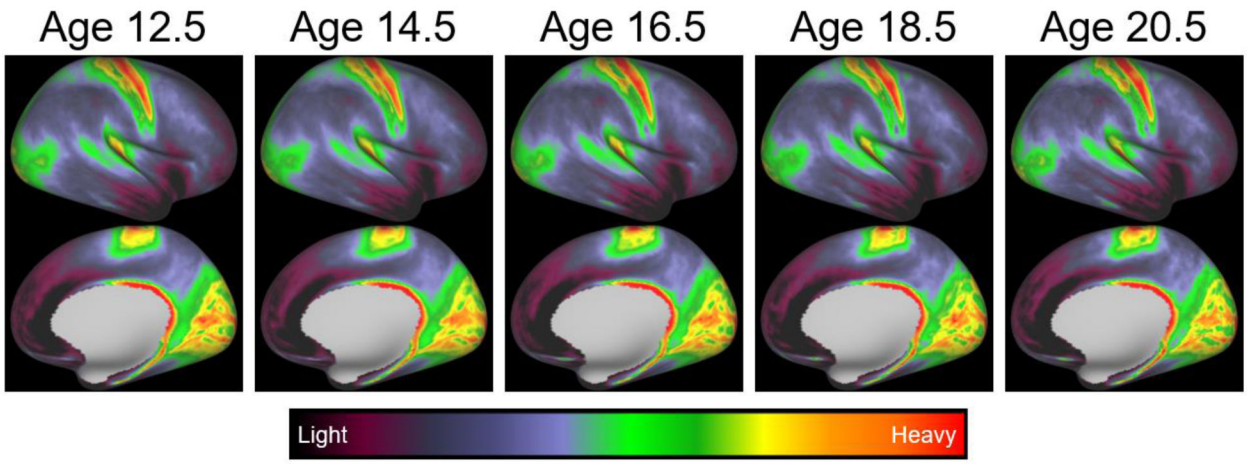

Figure 5.

The normalized myelin content is displayed on the averaged (inflated) brain surface for different adolescent age groups. Blue/black colors represent lightly myelinated regions and yellow/red colors show heavily myelinated regions. The images confirm our previous finding, i.e., they show greater gains in normalized myelin content in area 4 and smaller gains in area 23c and p24.

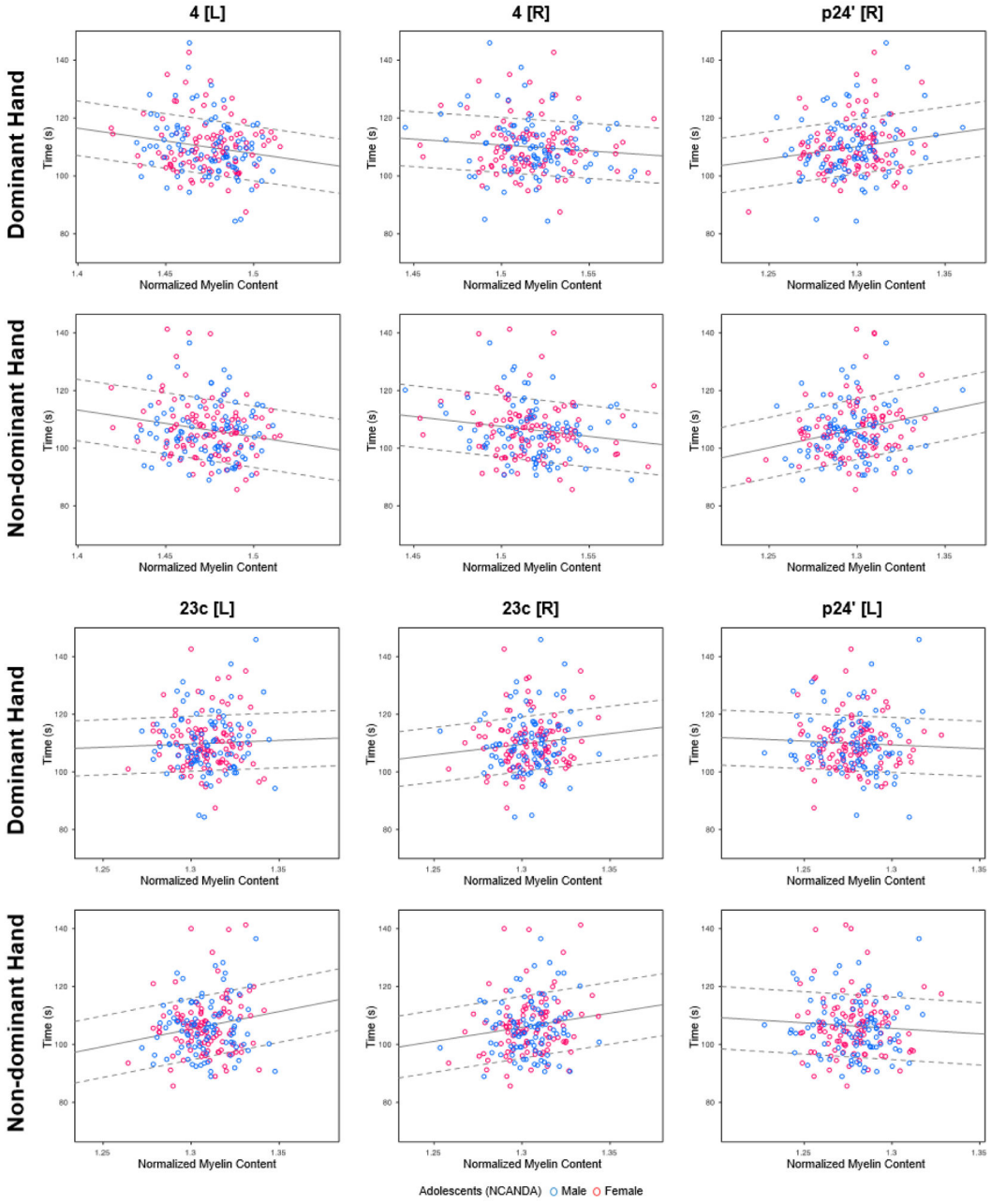

Figure 6.

Correlation tests for the *normalized* myelin content and Grooved Pegboard Test scores (total time in seconds) for NCANDA adolescents. Shorter performance time represents better performance. Plots between the *normalized* myelin content and grooved pegboard time performed by dominant (top row) and non-dominant (bottom row) hands are shown for areas 4, 23c, and p24'. Both myelin content and pegboard scores are the residuals with respect to age. Blue circles represent male and red represent female adolescents; the fits of the general linear regression are in gray.

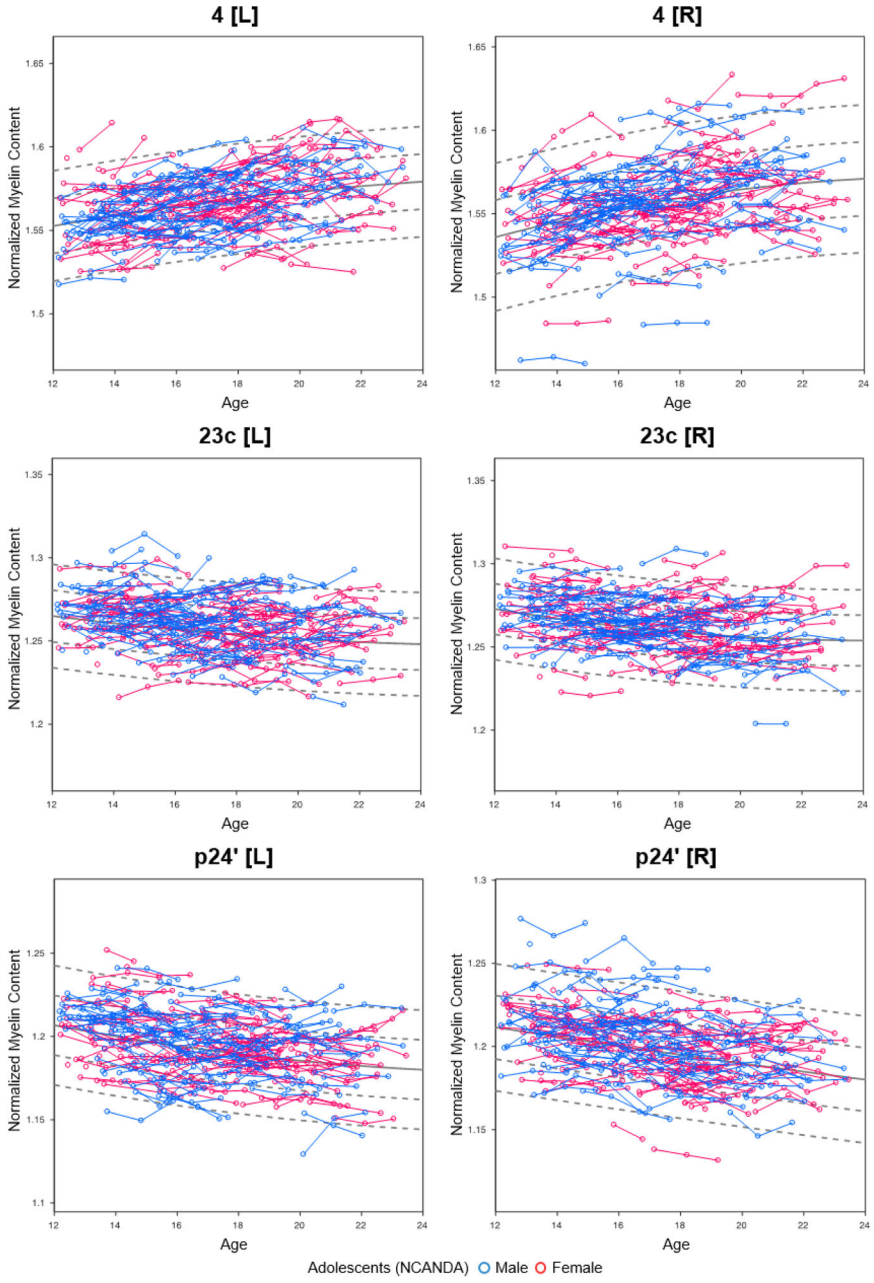

Figure 7.

Longitudinal *normalized* myelin content for adolescents (NCANDA) based on the longitudinal approach. Longitudinal plots of areas 4, 23c, and p24' are shown for left [L] and right [R] hemispheres. In each plot, blue circles stand for male and red for female adolescents. Visits are connected for each subject and the fits of the linear mixed effects model with +/− 1 and 2 SD are drawn in gray lines. The horizontal axes represent age (in years) and vertical axes the *normalized* myelin content.

Table 1

Group demographics for adolescents (NCANDA) and young adults (HCP)

		NCANDA Baseline		*NCANDA 2-year Follow-up*		*HCP Baseline*	
		Male	**Female**	**Male**	**Female**	**Male**	**Female**
Participants	**N**	108	118	91	94	264	422
Age (years)	**mean**	15.9	16.4	18.1	18.6	27.7	29.6
	SD	2.5	2.6	2.4	2.6	3.7	3.6
Site[†] **Self-declared**	**P/O**	41/67	49/69	32/59	37/57	N/A	N/A
Ethnicity	**N**	108	118	91	94	262	414
Caucasian		90	93	77	77	187	299
African-American		8	14	6	8	50	82
Others		10	11	8	9	25	33
Handedness[‡]	**L/R/A**	8/84/16	6/96/16	8/70/11	5/76/13	16/214/34	25/366/31

[†] NCANDA collection sites: P=University of Pittsburgh, O=Oregon Health and Science University

[‡] L=left, R=right, A=ambidextrous

Table 2

Cross-sectional age effects with respect to the *normalized* myelin content for adolescents (NCANDA) and young adults (HCP)

		NCANDA Baseline		***HCP Baseline***	
ROI	**Hemi**	**β_{age}**	**P**	**β_{age}**	**P**
4	L	0.0026	**< 0.001**	0.0016	**0.003**
4	R	0.0033	**< 0.001**	0.0014	0.156
23c	L	−0.0020	**< 0.001**	−0.0007	1.000
23c	R	−0.0023	**< 0.001**	−0.0018	0.056
p24'	L	−0.0026	**< 0.001**	−0.0015	0.096
p24'	R	−0.0028	**< 0.001**	−0.0019	**0.002**

P values are marked bold if P < 0.01

Table 3.

Pearson correlation (r-value) between *normalized* myelin content and Grooved Pegboard Test scores of NCANDA adolescents

		Dominant Hand		***Non-dominant Hand***	
ROI	**Hemi**	**r**	**P**	**r**	**P**
4	L	−0.175	**0.009**	−0.164	**0.013**
4	R	−0.102	0.078	−0.153	**0.011**
23c	L	0.038	0.327	0.170	**0.011**
23c	R	0.115	0.066	0.135	**0.027**
p24'	L	−0.047	0.248	−0.060	0.206
p24'	R	0.168	**0.013**	0.226	**0.001**

P values are marked bold if $P < 0.05$

Table 4.

Multiple Mediation Model for 4 [L] and p24' [R] tests for age, *normalized* myelin content, and Grooved Peaboard Test scores for NCANDA adolescents

ROI	Hemi	Path a_x		Path b_x		Path c_M (direct effect)			Path $a_x b_x$ (indirect effect)		
		β_a	P	β_b	P	β_c	P	β_n	$\beta_a \cdot \beta_b$	P	β_n
Dominant Hand											
Path d (total effect, Unmediated Model): $\beta_d = -1.283$, $P < 0.001$											
4	L	0.005	**< 0.001**	−71.88	**0.019**	−0.743	**0.006**	58%	−0.356	**< 0.001**	28%
p24'	R	−0.003	**< 0.001**	67.50	**0.042**				−0.184	**< 0.001**	14%
Non-Dominant Hand											
Path d (total effect, Unmediated Model): $\beta_d = -1.387$, $P < 0.001$											
4	L	0.005	**< 0.001**	−65.96	**0.042**				−0.327	**< 0.001**	24%
p24'	R	−0.003	**< 0.001**	113.56	**0.007**	−0.750	**0.013**	54%	−0.310	**< 0.001**	22%

P values are marked bold if $P < 0.05$. The Grooved Pegboard Test score is the total time in seconds to complete the test; shorter time indicates better performance. The normalized β_n value is the ratio between β value of an effect according to the mediation model divided by β_d, the β value of the direct (unmediated) effect between age and the pegboard score.

Table 5.

Longitudinal age effects of *normalized* myelin content for adolescents (NCANDA)

		Linear		*Quadiratic*	
ROI	**Hemi**	β_{age}	**P**	β_{age2}	**P**
4	L	0.0053	**0.004**	−0.00008	0.096
4	R	0.0089	**< 0.001**	−0.00017	**0.004**
23c	L	−0.0041	**0.012**	0.00008	0.105
23c	R	−0.0061	**< 0.001**	0.00013	**0.001**
p24'	L	−0.0061	**< 0.001**	0.00011	**0.022**
p24'	R	−0.0034	**0.041**	0.00002	0.630

P values are marked bold if P < 0.05. The linear and quadratic age effects of longitudinal myelin content tested with the linear mixed effects model. The slope model tested the linear age effects of the slope in percent (%/year) for longitudinal myelin changes.